THE UNIVERSITY OF CALGARY

Fiber Optic Current Sensor Network

by

Sandeep Goyal

A THESIS

SUBMITTED TO THE FACULTY OF GRADUATE STUDIES

IN PARTIAL FULFILLMENT OF THE REQUIREMENTS FOR THE

DEGREE OF MASTER OF SCIENCE

DEPARTMENT OF ELECTRICAL AND COMPUTER ENGINEERING

CALGARY, ALBERTA

SEPTEMBER, 1997

0-612-24716-3

ABSTRACT

With the commercial use of optical current sensors becoming a reality it will be highly beneficial for many applications if multiple sensors can be networked and have a single transceiver unit. An all fiber optic current sensor network is developed which uses a single detection scheme for current sensing.

Several network topologies and multiplexing approaches are presented and compared and based upon such comparisons a two sensor passive star network using time division multiplexing is adopted for use in the project. The transmitter to send the light pulses and receiver to detect the pulses and display them in a user friendly way have been designed and built.

This practical fiber optic current sensor network is used to carry out the experimental investigations and according to the data the proof of concept FOCSNET has been remarkably successful in differentiating and measuring the D.C. currents present in two 3M sensors simultaneously.

ACKNOWLEDGEMENTS

I would like to express my sincere gratitude to my Supervisor, Dr. Dave Irvine-Halliday for his valuable support, encouragement, suggestions and constructive criticism throughout this project.

I am also very grateful to Mr. Rob Thomson and Mr. John Shelley for their truly invaluable help and technical support throughout the duration of this project. Their assistance has gone a very long way in making this project a success.

Special thanks to Dr. Ed Nowicki for his constant support and advice, Mr. Patrick Walsh for helping set up the power supply facilities for the large current experiments and Mr. Dave Clegg of TRLabs, Edmonton for his unselfish help in building the laser and pragmatic advice on many occasions.

I wish also to take this opportunity to very thankfully acknowledge the immense contribution by Dr. Mike Messerly of 3M Inc. in providing us with the two optical fiber current sensors and the single mode fiber for use in this project.

Also, I am very thankful to the Department of Electrical and Computer Engineering for their help and NSERC for their generous funding of the entire project.

Finally, I would like to thank all my friends and colleagues for their continuous support and especially Andres Canalizo.

CONTENTS

LIST OF TABLES

LIST OF FIGURES

LIST OF SYMBOLS

A_x	amplitude of x-axis orthogonal component
A_y	amplitude of y-axis orthogonal component
α	attenuation factor of the system
α_s	splice loss
C_{P1}	couplers between the transmitter and the sensors
C_{P2}	couplers between the sensors and the receiver
c	velocity of light in free space
$dn/d\lambda$	dispersion of the medium
Δf	noise equivalent bandwidth
$\vec{E}$	electric field vector of polarized wave
E_x	electric field vector of x-axis orthogonal component
E_y	electric field vector of y-axis orthogonal component
e	charge on electron
e_0/m_0	specific charge of the electrons
γ	magneto-otical constant
H	magnetic field intensity
I	current present in the conductor
I_{amp}	op-amp noise current
I_d	dark current
I_{in}	op-amp input noise current

I_p	photo current
I_s	shot noise current
I_t	thermal noise current
J	intensity of light at input of first polarizing fiber
J_{in}	intensity of light at output of first polarizing fiber
J_{out}	intensity of light at output of second polarizing fiber
k	Boltzmann's constant
L	length of the optical path
$L1$	length of the first fiber
$L2$	length of the second fiber
L_{CI}	excess loss of the coupler
L_{IT1}	tap ratio loss of coupler to sensor (90:10)
L_{SC}	excess loss of the Star coupler
L_{T1}	tap ratio loss of coupler on the transmitting fiber (10:90)
L_{T2}	tap ratio loss of the couplers on the receiving fiber (50:50)
L_{TS}	tap ratio loss of the Star coupler
λ	optical wavelength
m	mass of electron
N	number of turns of optical path around the conductor
n	refractive index of the medium
n_+	refractive index of the right circularly polarized component of the light

n_-	refractive index of the left circularly polarized component of the light
Ω	Faraday rotation angle
ω	angular frequency
ω_L	Larmor frequency
ϕ_x	phase angle of x-axis orthogonal component
ϕ_y	phase angle of y-axis orthogonal component
R_f	feedback resistance
SNR	signal to noise ratio
T	temperature
t_{L1}	time taken by leading edge of the first pulse to reach the receiver
t_{L2}	time taken by leading edge of the second pulse to reach the receiver
t_p	pulse duration
t_{sep}	separation between the two pulses
V	Verdet constant
V_{amp}	op-amp noise voltage
V_{in}	op-amp input noise voltage
V_{noise}	total system noise voltage
V_s	shot noise voltage
V_t	thermal noise voltage

CHAPTER 1

INTRODUCTION

1.1 Background

Electrical current measurements are of fundamental importance in power networks and particularly where they are used for relaying, metering, control and monitoring purposes. While the conventional current transformers (CTs) have performed on the whole quite well since the late 1800's, performance limitations and other failures[1] have provided an impetus towards using other methods.

Recent demands for higher voltage electric power systems have led to an increase in the size and cost of the conventional CTs. The saturation of the iron core under fault current[2] and the low frequency response of the conventional CTs make it difficult to obtain accurate current signals under transient conditions and it also reduces the dynamic range of the CT. Moreover, with digital control and protection systems being introduced into power systems, the conventional CTs have caused further difficulties, as they are likely to introduce electro-magnetic interference (EMI) through the ground loop into the digital systems. The elimination of EMI in the current measuring system is therefore required.

1.2 Brief Review of the Optical Current Sensor

In recent years it has been recognized that there are significant advantages to using optical methods for measuring electrical currents in various applications[3, 4]. The optical current sensor, or optical CT, with its excellent features such as very much smaller size and weight than the conventional CTs, elimination of electromagnetic interference in current measurements, extension of dynamic range and frequency response, and the provision of an insulated optical link extending from the CT to the signal processing unit or relaying system[5], provides a solution to the above mentioned limitations of conventional CTs. One can see that optical current-sensing techniques are sorely needed by the power industry and they will be widely used once developed. This is a vast potential market with huge social and economic benefits.

An optical current sensor measures the electric current by means of the Faraday Magneto-optic effect which was first observed by Michael Faraday 150 years ago. The Faraday effect is the phenomenon whereby the orientation of polarized light rotates under the influence of a magnetic field and the degree of rotation is proportional to the strength of the magnetic field component in the direction of the optical path.

In an optical CT system a sensor element is placed on the electrical conductor where the measurement is to be made and laser light is injected into it from a remote transmitter station through either an optical fiber or free space[6, 7, 8]. The incident light is modulated by the sensor and then returned to an optical receiver station where the modulation is detected, quantified and translated into a current value. Because of the Faraday effect the sensor alters the polarization state of the laser beam and this change can be detected by using the two detector method or the single detector method[9, 10]. In the two detector system the change in the polarization state is detected using a Wollaston prism and a pair of photodetectors arranged to measure orthogonal polarization components[11]. In the single detector system the intensity of the light beam is altered by the change in the polarization state and this variation in the intensity is detected using a single photodetector at the receiver end.

A majority of optical CT systems have utilized the two detector approach in order to improve the signal to noise ratio. Even though the dual detector approach provides superior rejection of common mode noise it is more costly and difficult to implement relative to the single detector system, especially in an all fiber system[12].

The designs of optical CTs to date have fallen into two categories. bulk glass type and fiber optic type. In the bulk glass design[13. 14. 15. 16. 17] an optical glass prism is used as the sensing unit and an optical fiber is used to transmit the optical signal. The optical glass prism is formed around the conductor to allow the optical beam to go around the conductor to pick up the Faraday rotation. The bulk optic approach requires lenses, polarizers and highly stable assemblies for joining the sensing element to the rest of the optical system. Furthermore. increasing the number of optical turns (thus increasing the sensor's response to smaller currents) is difficult and costly. With the fiber optic approach[18. 19. 20. 21. 22]. the optical fiber is wound around the current carrying conductor as a coil to pick up the Faraday rotation change. The optical fiber is thus used both to sense the electric current and to transmit the optical signal. Due to the very simple structure (just a few turns of fiber) and the potential cost reduction, small size and reliability advantages of an all fiber optic system, special attention is being paid to this field.

1.3 Fiber Optic Current Sensor Network (FOCSNET)

Using an all fiber optic approach it is much simpler to design a sensor network having a single transmitter and receiver and have multiple sensors placed at different locations networked together, whereas in the bulk optic approach it is extremely complex and difficult to build such a network. The fact that the sensor technology has reached the level where the fiber optic sensors are commercially available enables the building up of not only the single point sensor systems, but a whole network of sensors driven by a single optical source. A key advantage of, and motivation for, sensor multiplexing is a reduction in the overall cost per sensor, because all sensor elements are powered and interrogated by a single transceiver unit. It is expected that a major thrust for the greater application of fiber optic sensors will arise from the need to install an increasing number of sensors in applications requiring the use of multiple sensors e.g. in the electrical power industry.

Different techniques can be used to build such a network[23, 24] like frequency division multiplexing (FDM), time division multiplexing (TDM) and wavelength division multiplexing (WDM). The multiplexing method may be said to be passive, if only passive sensor and interconnection elements are used (i.e., there is no need for external electrical power). Fiber optic sensors are intrinsically suited to such passive multiplexing schemes.

In the FDM technique every sensor of the network is assigned a frequency channel within which the sensor signal may be modulated in amplitude or frequency by the corresponding measurand[23, 24, 25]. WDM is principally a special case of FDM, but due to the enormous bandwidth of fiber optic signals it is considered as a distinct multiplexing method. Here, a separate wavelength is assigned to each sensor channel of the network[23, 26]. However, FDM requires a highly accurate and complex electronic processing unit and WDM requires very sensitive and selective optical components.

The TDM approach consists of launching short light pulses into the network and detecting the differentially delayed returning pulses caused by the different fiber lengths to each sensor[23, 24].

Distributed sensing schemes like optical Time Domain Reflectometery (OTDR) where the fiber itself acts as the sensor have also been used[23, 26, 27]. OTDR utilizes an optical radar concept to measure the backscatter power versus time characteristics when a light pulse is launched into the fiber. Also work has been done on coherence multiplexing of sensors where a short coherence length continuous optical source is used[28, 29]. The main principle behind this technique is that the delays in the sensor array are arranged so that the optical signal returns are mutually incoherent and therefore do not interfere coherently with one another. The signal from each sensor can then be retrieved separately by matching the delay in the receiving interferometer.

Keeping firmly in mind the overall complexity of design and resource limitations the TDM approach appears to be a more pragmatic choice than the others.

1.4 Thesis Outline

The aim of this thesis is to investigate the feasibilty of an all fiber optical current sensor network. Further details about FOCSNET are described in the following chapters:

In Chapter 2 the polarization phenomenon of light is discussed and the Faraday Magneto-optic effect is analysed.

In Chapter 3 the types of networking techniques considered are presented. An analysis of the pros and cons of using different networking topologies is carried out. leading to the choice of topology used in FOCSNET.

In Chapter 4 the design of FOCSNET is explained in detail. It can be broadly divided into three categories: Transmitter, Receiver and Optics. In the Optics section various types of optical fibers and their properties are explained in detail. The Receiver section can be subdivided into an Electronics part which includes the Photodiode and Operational Amplifiers, and the Digital part which includes the Analog to Digital converter. the Field Programmable Gate Array (FPGA) and the Digital Signal Processor.

Chapter 5 includes the expected performance of the system. an in-depth study of various causes that may affect the system is done and a Signal to Noise analysis is presented.

Chapter 6 contains the experimental investigation and results. A detailed examination of the procedural set up and the results obtained is carried out and it is followed by a discussion on the possible sources of errors.

Finally. the conclusions and future work are given in Chapter 7.

CHAPTER 2

OPTICS

2.1 Polarization

The polarization of light was first discovered by a Danish professor Erasmus Bartolinus and described in a publication in 1669[30]. This reference concerned the refraction seen in a crystal called Iceland Spar, now called Calcite. After extensive work on this phenomena by Hugens, Malus, Brewster, Young and others, the theory of polarization is now generally considered well developed.

A beam of light consists of many waves with each wave having its own electric field component. Normally the orientations of these electric field components are randomly distributed and such a light is called unpolarized light. A polarized beam of light is one in which the electric field components of all the waves have similar orientation.

The orientational characteristics of the electric vector representing the polarized light determine the state of polarization (SOP) of the wave[31]. If the incoming wave is seen from the direction of propagation i.e. the z-axis, the locus of the tip of the electric vector is a measure of the polarization. The angular orientation of this locus is known as orientation of the wave. If the locus is a straight line the wave is said to be linearly polarized and it is called circularly polarized light if the locus is a circle. The circularly polarized light is further divided into right or left circularly polarized light depending upon the direction of the circular helix. If it is clockwise then it is known as right circularly polarized light and if anti-clockwise then left circularly

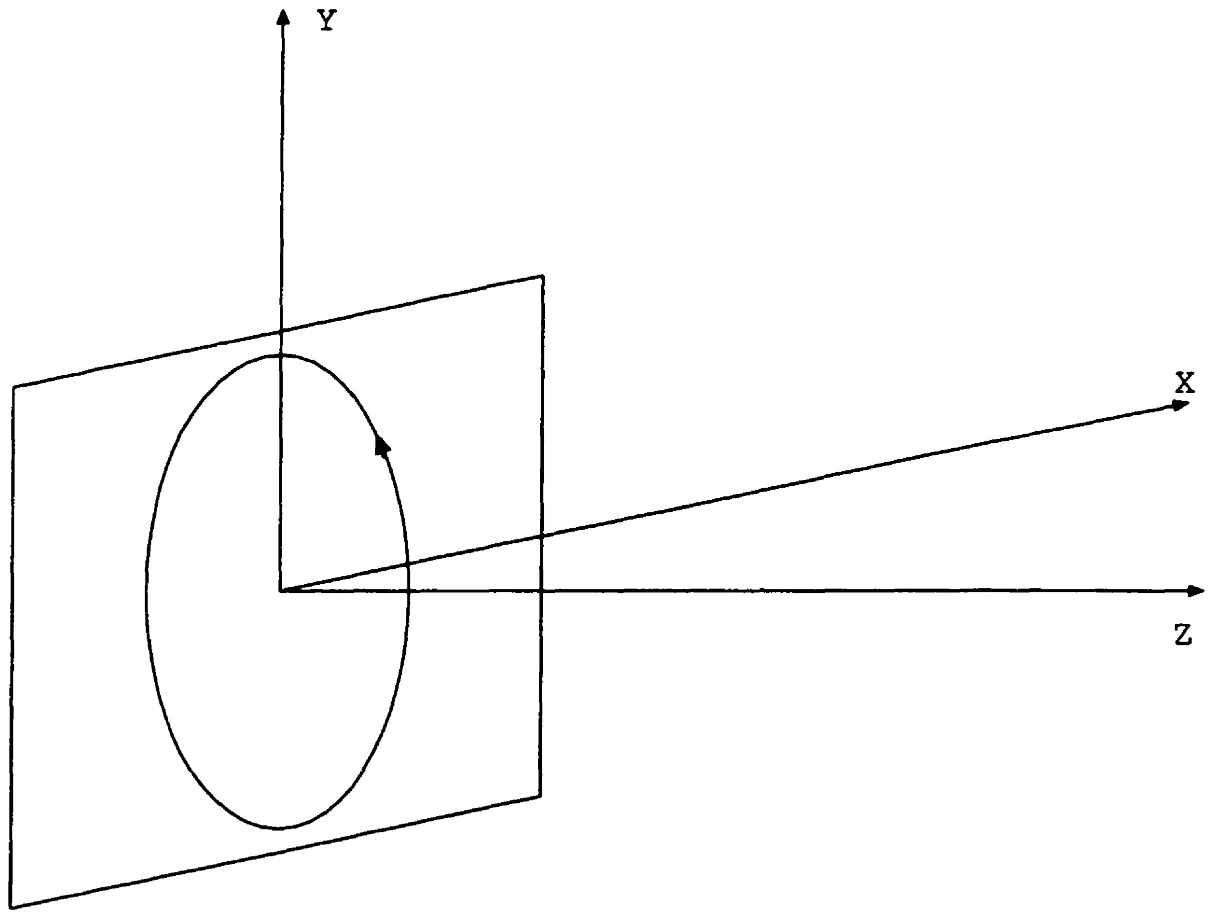

Figure 2.1. Sectional Pattern of left elliptically polarized light

polarized light. Fig. 2.1 shows the sectional pattern of a left elliptically polarized wave viewed towards the source having an orientation of 90° from the x-axis.

Any vector representing a polarized light beam can be resolved into a pair of mutually perpendicular or orthogonal components of the electric field travelling along the direction of propagation of light[31]. In other words, the electric field vector of the polarized light is a vector sum of these two orthogonal components. Thus the intensity, the orientation and the type of polarized light depends upon these orthogonal components. These components lie along the x and y axes.

If the two components are in phase then the resultant wave is linearly polarized. The orientation of this linearly polarized light depends upon the relative amplitudes of the two components and if their amplitudes are equal then the orientation is at 45°. The orientation of polarized light is measured conventionally with respect to the x-axis. If A_x and A_y are the amplitudes of the x and y orthogonal components respectively, then the orientation of resultant linearly polarized light can be given by $tan^{-1}(A_y/A_x)$.

If the two orthogonal components are equal in amplitude and are 90° out of phase then the resultant wave is said to be circularly polarized. Circularly polarized states are distinguished by the sense of rotation of the vector. For example, when the resultant vector rotates clockwise when viewed towards the source it is called right circularly polarized light. Circularly polarized light does not have any orientation as such and it is described by just its amplitude and sense of rotation.

For other cases when the two components have unequal amplitudes and have a phase difference, or have equal amplitudes but a phase difference other than 90°, the result is elliptically polarized light. Generally, all the polarized light can be termed as elliptically polarized with linear and circular polarization being its special cases. Fig. 2.2 shows in detail the effect that the amplitudes and the phase difference of the two orthogonal components have on the overall state of polarization of the light wave[32].

Sectional Pattern of Polarized Wave	Sectional Patterns of Orthogonal Components	Orientation (in degrees)	Phase Difference between the two components	Type of Polarized Light
	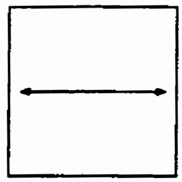	0	0	Linear
	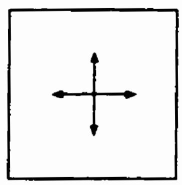	45	0	Linear
	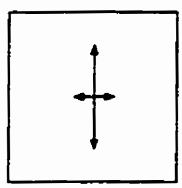	70	0	Linear
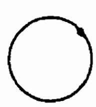	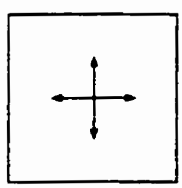	-	90	Right Circular
	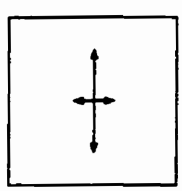	90	90	Left Elliptical

Figure 2.2. Relationship between orthogonal components and type of polarization

2.2 The Jones Calculus

Many scientists such as Jones, Stokes and Mueller have developed mathematics to represent the polarized light and its interaction with optical systems[31, 32]. Detailed discussion about the Jones Calculus is presented in this section.

In 1941, R.C. Jones[33] determined that polarized light could be represented by a 2x1 column vector which is known as the Jones vector. Each element of the Jones vector describes one component of the electric vibration at the given location. The first (upper) element indicates the amplitude and phase of the X-component and the second (lower) element does the same for the Y-component.

Assume there is a beam of polarized light (not necessarily linearly polarized light), which can be considered as a plane wave travelling with the speed of light, c, and in the direction of z-axis. Its electric field vector $\vec{E}$ can be specified[15] in terms of two orthogonal components E_x and E_y, with amplitude A_x and A_y, and initial phase angle ϕ_x and ϕ_y respectively, such that

$$E_x = A_x cos[\omega(t - \frac{z}{c}) + \phi_x] = Real\ part\ of\ \left[A_x exp\ i[\omega(t - \frac{z}{c}) + \phi_x]\right] \tag{2.1}$$

and

$$E_y = A_y cos[\omega(t - \frac{z}{c}) + \phi_y] = Real\ part\ of\ \left[A_y exp\ i[\omega(t - \frac{z}{c}) + \phi_y]\right] \tag{2.2}$$

When $|\phi_x - \phi_y| = 90^\circ$ and $A_x = A_y$, $\vec{E}$ is circularly polarized. When $\phi_x - \phi_y = 0$, $\vec{E}$ is linearly polarized. In a general case $\vec{E}$ is elliptically polarized. The above equations can be rewritten in a different form as follows,

$$\begin{bmatrix} E_x \\ E_y \end{bmatrix} = \begin{bmatrix} A_x e^{i\phi_x} \\ A_y e^{i\phi_y} \end{bmatrix} e^{i[\omega(t-z/c)]} \tag{2.3}$$

Alternatively, $\vec{E}$ can be represented as a column vector which is called the Jones Vector

$$\begin{bmatrix} E_x \\ E_y \end{bmatrix} = \begin{bmatrix} A_x e^{i\phi_x} \\ A_y e^{i\phi_y} \end{bmatrix} \tag{2.4}$$

For example.

$\begin{bmatrix} 1 \\ 0 \end{bmatrix}$ is a linearly polarized light with the orientation of the x-axis.

$\begin{bmatrix} 0 \\ 1 \end{bmatrix}$ is a linearly polarized light with the orientation of the y-axis.

$\frac{1}{\sqrt{2}} \begin{bmatrix} 1 \\ 1 \end{bmatrix}$ is a linearly polarized light which is 45° oriented with both the x-axis and y-axis, and

$\begin{bmatrix} 1 \\ i \end{bmatrix}$ is a right-circular polarized light.

Jones also found that a polarization device can be represented as a 2x2 matrix which is known as the Jones matrix. When the polarized light is passed through the polarization device, the output light can be represented as another column vector which is the product of the Jones matrix of the device and the Jones vector of the input light as shown below :

$$\begin{bmatrix} E_{2x} \\ E_{2y} \end{bmatrix} = \begin{bmatrix} J_{11} & J_{12} \\ J_{21} & J_{22} \end{bmatrix} \begin{bmatrix} E_{1x} \\ E_{1y} \end{bmatrix} \tag{2.5}$$

In general, the four elements of the Jones matrix, J_{11}, J_{12}, J_{21}, and J_{22}, are complex and depend on the device[15]. For example, a quarter wave plate which is an important optical component can provide a 90° phase difference between the two orthogonal components of the polarized light. If the orientation angle of the quarter-wave plate is 45° then its Jones matrix is

$$J = \frac{1}{\sqrt{2}} \begin{bmatrix} 1 & i \\ -i & 1 \end{bmatrix} \tag{2.6}$$

and the Jones vector for the input light is $E_{in} = \begin{bmatrix} 0 \\ 1 \end{bmatrix}$

Therefore the output light which can be represented as a product of these two is

$$E_{out} = \frac{1}{\sqrt{2}} \begin{bmatrix} 1 & i \\ -i & 1 \end{bmatrix} \begin{bmatrix} 0 \\ 1 \end{bmatrix} = \frac{1}{\sqrt{2}} \begin{bmatrix} 1 \\ i \end{bmatrix} \tag{2.7}$$

which is a right-circular polarized light.

The Jones matrix for any material which rotates the polarized light by an angle θ is given by

$$R = \begin{bmatrix} cos\theta & sin\theta \\ -sin\theta & cos\theta \end{bmatrix} \tag{2.8}$$

2.3 Faraday Magneto-optic Effect

In 1845 Michael Faraday discovered that when polarized light is propagated through an optically active material in a direction parallel to the applied magnetic field, its plane of polarization was rotated and this rotation angle was proportional to the intensity of the magnetic field[34]. This is known as the Faraday effect and the rotation is generally given by the empirical law

$$\Omega = V \int_0^L \vec{H}.d\vec{l} \tag{2.9}$$

where,

Ω - Angle of rotation,

V - Verdet constant of the material (rad/ampere-turn),

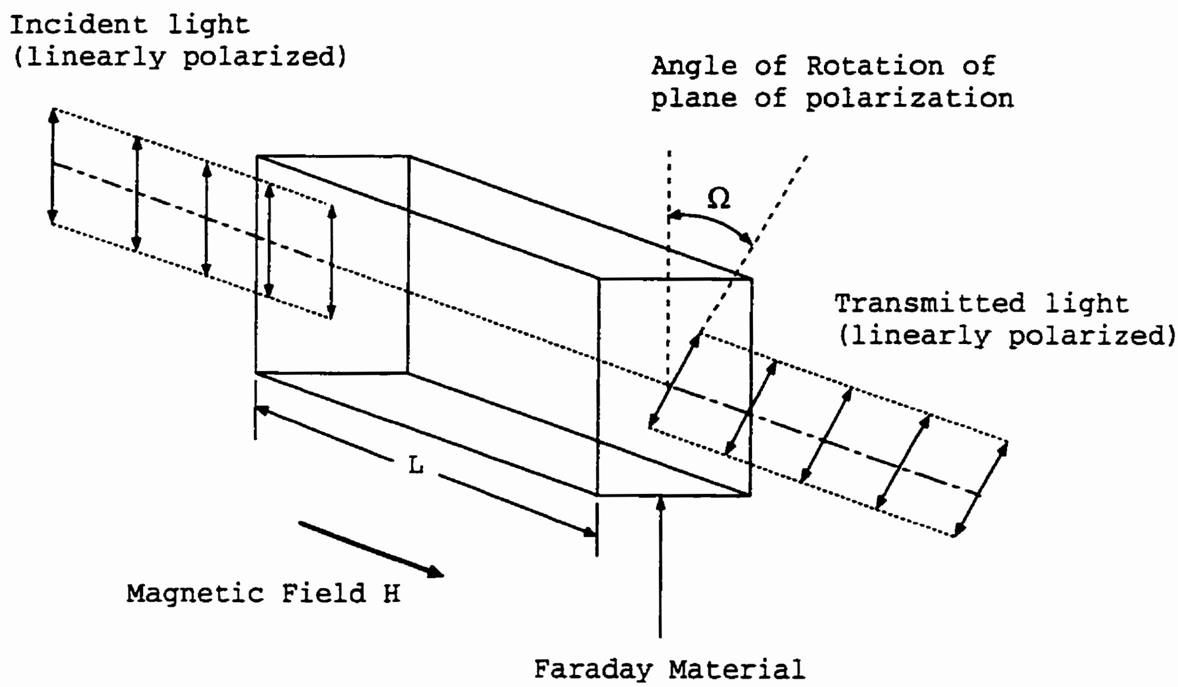

Figure 2.3. Concept of Faraday Effect

H - Magnetic field intensity, and

L - Length of the optical path.

If the magnetic field is uniform and the optical path is going along the same direction as the magnetic field then the above relation can be simplified as

$$\Omega = VHL \tag{2.10}$$

When the propagation direction differs from the magnetic field direction by an angle ϕ, the rotation is given by

$$\Omega = VHLcos\phi \tag{2.11}$$

When the polarized light encircles a current carrying conductor through a magneto-optical material like optical fiber then according to Ampere's Law the Faraday rotation[16] can be given as

$$\Omega = VNI \tag{2.12}$$

where.

N - Number of turns of the optical path around the conductor. and

I - Current carried by the conductor.

The Verdet constant is generally described by the microscopic theory: it is temperature. wavelength. and sometimes field-dependent and it is different for different materials. The dependence of the Verdet constant on the wavelength and the refractive index is expressed as[15]

$$V = \gamma \frac{e_0}{m_0} \frac{\lambda}{2c} \frac{dn}{d\lambda} \tag{2.13}$$

where.

V - Verdet constant of the material.

γ - magneto-optical constant.

e_0/m_0 - specific charge of the electrons,

c - velocity of light.

λ - wavelength.

n - refractive index of material at wavelength λ, and

$dn/d\lambda$ - dispersion.

Thus higher the dispersion of the material, the larger the Verdet constant.

The Faraday effect is a dispersion effect and can be understood in terms of the space anisotropy introduced by the magnetic field[16]. As the effect of the magnetic field upon the right and left circularly polarized components is different the refractive indices and the propagation constants are also different for each sense of polarization and a rotation of the plane of polarization of the linearly polarized wave is observed. If there is absorption in the medium, then the absorption coefficient will also be different for each sense of circular polarization and the emerging beam will then be elliptically polarized.

In 1825, Fresnel showed that for natural optical rotation the plane polarized wave could be considered as right and left circularly polarized waves travelling through the medium at different velocities. The rotation of the plane of polarization for light passing through a material of length L is given by[16, 31]

$$\Omega = (\omega L/2c)(n_- - n_+) \tag{2.14}$$

where ω is the angular frequency, n_+ and n_- are the refractive indices of the right and left components respectively, and c is the velocity of light. Since this description does not depend on the manner in which the differing velocities arise it is also applicable to magnetic rotation.

Rotation arises through the coupling of radiation with the electrons or bound oscillators[16]. The magnetic field can be taken into account by using a moving coordinate system which precess the the Larmor frequency $\omega_L = eH/2mc$, where e and m are, respectively, the amplitude of the charge and the mass of the electron. The two components of the radiation then have the angular frequencies $\omega - \omega_L$ and $\omega + \omega_L$. From the equation for the rotation given above, Ω is then given by

$$\Omega = [n(\omega - \omega_L) - n(\omega + \omega_L)]\omega L/2c = (\omega L \omega_L/c)(dn/d\omega) \tag{2.15}$$

which is called the Becquerel equation[16].

All dielectric materials exhibit this Faraday effect to some extent. In particular it is found that glasses and silica, the materials from which optical fibers are made, have measurable Verdet constants. As silica has a relatively small Verdet constant it is necessary to have a strong magnetic field or a large amount of current in the conductor in order to measure the Faraday effect on optical fibers.

2.4 Polarization and Fiber Optics

The polarization state of light traveling through a medium can be influenced by stress within the medium and this can present problems with ordinary single mode fiber[35, 36, 37]. When a normal fiber is bent or twisted stresses are induced in the fiber and these stresses in turn change the polarization state of light traveling through the fiber[38, 39]. Furthermore if the fiber is subjected to any external perturbations like those due to changes in temperature then the final output polarization will vary with time. This is true for even short lengths of fiber and is undesirable in many applications which require a constant output polarization from the fiber.

Polarization maintaining fibers (PM fibers) have been developed to solve this problem. These fibers are also known as High Birefringent or Hi-Bi fibers and work by inducing a birefringence within the fiber core. Birefringence refers to a difference in the propagation constant of light traveling the fiber for the two orthogonal polarizations[31, 39, 40]. This birefringence breaks the circular symmetry in an optical fiber creating two principal transmission axes within the fiber known respectively as the fast and slow axes of the fiber. The high birefringence of these fibers prevents the coupling of power between the two orthogonal components. This results in very low noise and cross-talk and helps in maintaining the state of polarization of the light traveling through the fiber. Provided that the input light into a PM fiber is linearly polarized and oriented along one of these two axes then the output light from the fiber will remain linearly polarized and aligned with the principal axis even when subjected to external stresses.

Birefringence is created within a PM fiber either by forming a non-circular fiber core (shape induced birefringence), or by inducing constant stresses within the fiber with stress applying parts (SAP) (stress induced birefringence)[38, 39, 40]. An example of the shape induced birefringence is the elliptical core fiber. The optical losses of these types of PM fibers are generally high and the reason may be due to the large refractive index difference and imperfection of the core shape. On the other hand, the stress induced birefringent fibers such as bow-tie fibers and PANDA fibers exhibit low optical losses and low crosstalk levels by setting the buffer layer between the core and the stress applying parts (SAP)[40]. At present the most popular fiber type in the industry is the PANDA fiber which is of circular SAP type[39]. One advantage of PANDA fiber over most other fibers is that the fiber core size and numerical aperture is compatible with the regular single mode fiber and this ensures minimum losses in devices using both types of fibers. Fig. 2.4 shows a variety of polarization maintaining core/cladding structures presently used in the industry. The dashed lines in the drawings show the slow axis within each structure.

Polarizing fiber (PZ fiber) is a special type of PM fiber[40]. While in the PM fiber there is high birefringence between the two orthogonal modes in the PZ fiber one mode is driven to cut-off[41, 42]. At cut-off the mode ceases to be guided in

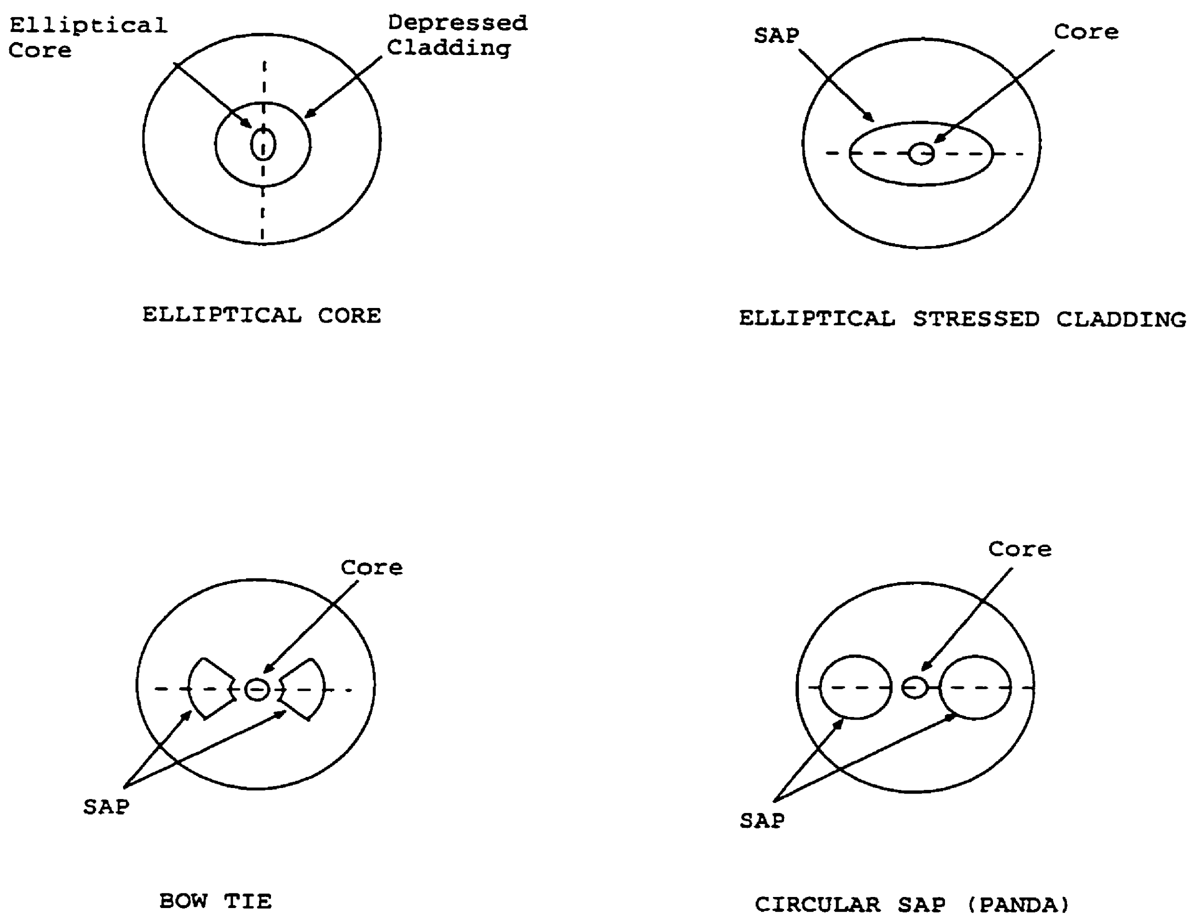

Figure 2.4. Some Polarization Maintaining Fiber Core Structures

the core region and it escapes into the cladding where its energy is lost. Normally, the light launched into the slow axis is guided inside the fiber and it emerges as linearly polarized light having the same orientation as that of the slow axis. Light launched into the fast axis is unguided and so it is driven to cut-off, thus no output light emerges from the fast axis. This means that the output light from the PZ fiber is linearly polarized in the direction of the slow axis irrespective of the nature and orientation of the input light. However the amplitude of the output light is a function of the relative difference between the orientation of the input light and that of the slow axis of the PZ fiber as shown in Fig. 2.5. If the input light is totally depolarized light then the amplitude of the output light is half that of the input light. Thus PZ fiber acts as a fiber polarizer.

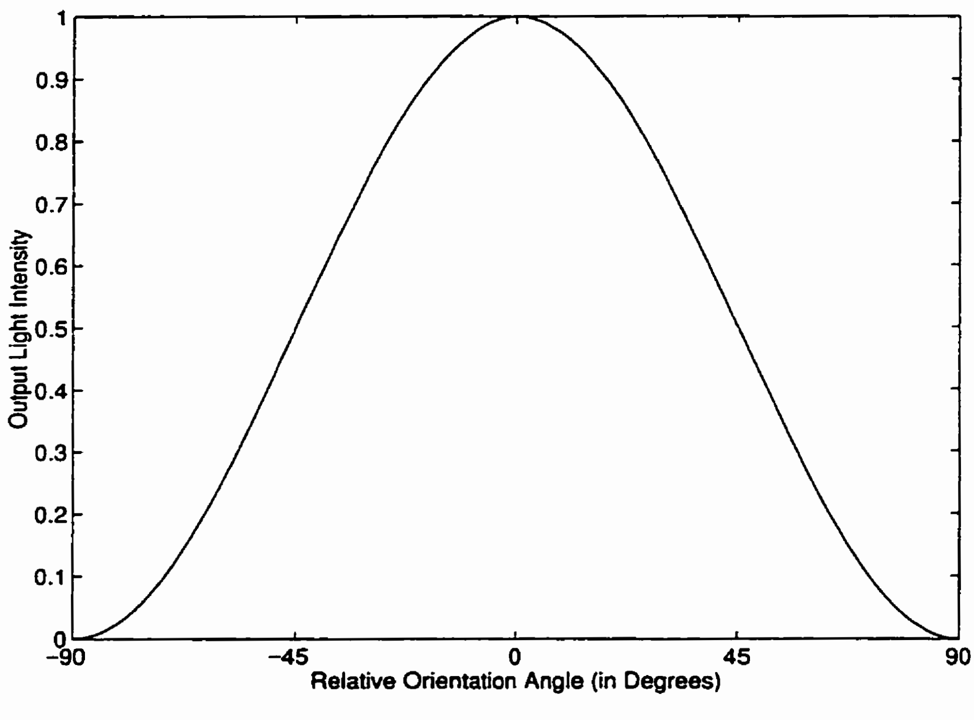

Figure 2.5. Output Light Intensity versus Relative Orientation Angle

2.5 The Sensing Coil

The plane of polarization of the polarized light inside the sensing fiber is rotated when it experiences the Faraday magneto-optic effect. The sensing fiber should have a very low birefringence for this rotation to take place as a high birefringent fiber may resist the magnetically induced circular birefringence of the Faraday effect. The phenomenon of difference in the velocities of the two oppositely handed circular polarizations traveling along the principal axis is known as 'circular birefringence'[31]. When fibers are carefully made they can have low linear birefringence; however, as the fiber is bent or comes under transverse pressure, the birefringence increases[43]. The linear birefringence interferes with the Faraday-induced rotation and even if present in small amounts it makes the Faraday rotation nearly unmeasurable[44]. Many approaches have been used by researchers and scientists for reducing the problems caused by linear birefringence in the fiber.

Early work to overcome the birefringence problem aimed at producing a low birefringence fiber by spinning the preform during fiber drawing to average the fast and slow birefringence axes[44]. However, when coiled, the fiber suffers from bend induced birefringence which can catastrophically reduce the electrical current sensitivity.

Another approach is to introduce high circular birefringence into the fiber or use a fiber with high intrinsic circular birefringence. Circular birefringence causes a rotation of the plane of polarization that merely adds to that caused by the Faraday effect. If the circular birefringence is sufficiently large then linear birefringence arising from bending or other effects has little effect[45].

Circular birefringence can be introduced into the fiber by torsional stress induced by twisting. However, it is effective only for relatively large coils with few turns[44, 45]. For small coils the twist necessary to achieve a useful effect often exceeds the breaking strength of the fiber. Further, the twist-induced circular birefringence is temperature dependent thereby introducing a stability problem. Several attempts have been made to make fiber with a high intrinsic circular birefringence by introducing large permanent levels of torsional stress locked into the fiber but these suffer from practical difficulties[44, 45].

In recent years, it has been shown that both the inherent and bend-induced linear birefringence can be substantially reduced by annealing the optical fiber at the temperatures in the range of 800°C[43]. Current sensors based on annealed coils offer better temperature stability than has been achieved with the other approaches. A further advantage is that annealed coils can be inexpensively produced from ordinary telecommunications fiber[45]. The principal difficulty is that the coils must be carefully packaged for protection and to minimize the sensitivity to vibration. The sensing coil used in this project was annealed in a ceramic mold and transferred to an identically shaped plastic holder[22].

CHAPTER 3

NETWORK DESIGN

3.1 Introduction

In a sensor network. at least two sensors. which may be discretely or continuously distributed in space according to a suitable topological pattern (linear array. star. ladder. ring). are operated and controlled by a single central optoelectronic terminal or transceiver unit. This requires a scheme to provide unambiguous sensor addressing (or multiplexing) and interrogation (or demodulation). The central terminal or transceiver is required to perform the following functions[23]:

- powering the network with an optical light flux of required intensity. spectral distribution. state of polarization (SOP). and temporal behaviour (continuous or modulated);
- detecting the part of the optical power that is modulated by the measurand's action in point sensor elements and sent back;
- identifying the information concerning the value of the measurands of the various point sensors by a suitable addressing, interrogation and decoding scheme;
- evaluating the separated individual sensor signals into electrical output signals that are calibrated against the particular measurands.

3.2 Multiplexing Techniques

The topology of a fiber optic sensor network is strongly determined by the desired method of sensor modulation and interrogation. The interrogation may be performed in the time and frequency or wavelength domain and these methods are referred to as Time Division Multiplexing (TDM), Frequency Division Multiplexing (FDM) or Wavelength Division Multiplexing (WDM), respectively. Distributed sensing systems like Optical Time Domain Reflectometery (OTDR) can also be used.

3.2.1 Time Division Multiplexing

This system consists of launching short light pulses into the network consisting of multiple point sensors distributed in space such that the returning pulses are delayed by time intervals given by $t_i = nL_i/c$, where L_i is the fiber link length of the ith sensor, n the core refractive index of the fiber, and c the free space velocity of light. At the detector the pulses arrive separated in time due to the different path lengths traveled to and from each sensor[23, 24]. They are then converted to electrical signals and the original signal decoded. The number of sensors that can be usefully multiplexed is governed by factors such as the pulse power, pulse width, repetition rate of the laser, the optical losses suffered in traversing the fiber and couplers, etc.

3.2.2 Frequency Division Multiplexing

In the FDM technique every sensor of the network is assigned a frequency channel within which the sensor signal may be modulated by the corresponding measurand[24, 25]. The most convenient form of frequency modulation is a linear fm ramp repeated at regular intervals. This waveform is either generated directly by a signal generator or indirectly by pulsing a surface accoustic wave (SAW) chirp filter. It is then amplified and applied to the laser or electro-optic modulator. The return signals from the sensors are then mixed with the original signal. Each return is separated in time from the original modulation by a definite time difference and this results in a fixed frequency difference from the original signal. This frequency difference is due to the nature of the linear fm ramp form of modulation. The different frequencies are then separated and the low frequency sensor modulation is recovered by detection and low pass filtering.

3.2.3 Wave Division Multiplexing

In this technique a separate wavelength is assigned to each sensor channel of the network. Wavelength Division Multiplexing is normally a multi-source concept. Light from a set of narrow-band sources (e.g. LEDs) is fed, via a combiner and a single input fiber, to the appropriate sensor of the network. The intensities modulated by the sensors are recombined and subsequently selected by a second demultiplexer and a detector array. Generally there is a crosstalk producing overlap between adjacent channels. Other contributions to crosstalk may come from scattering and mode coupling effects in fiber components in addition to any crosstalk within the interrogating optoelectronics. The quality of WDM components is characterized by such factors as channel separation, crosstalk and passband insertion loss.

Transferring this technology to the fiber optic sensor network, whilst in principle of interest, has yielded very few convincing experimental results[26]. The principal reason is that for widely spaced wavelengths (e.g. 850, 1300 and 1550 nm) where the wavelength separation components are simple to fabricate, the number of sensors which can be connected on the network is very limited. The complexity of the receiver for closely spaced wavelengths is currently beyond the cost constraints of most sensor systems.

3.2.4 Distributed Optical Fiber Sensing

The principal feature of a multiplexed network is that discrete sensors are attached to terminal points within the network and interrogated individually. In distributed sensor systems the fiber itself acts as a sensor and a spatially dependent signal is extracted from the sensor. The parameter to be measured stimulates measurand dependent coupling between the interrogating signal and the sensing channel. This

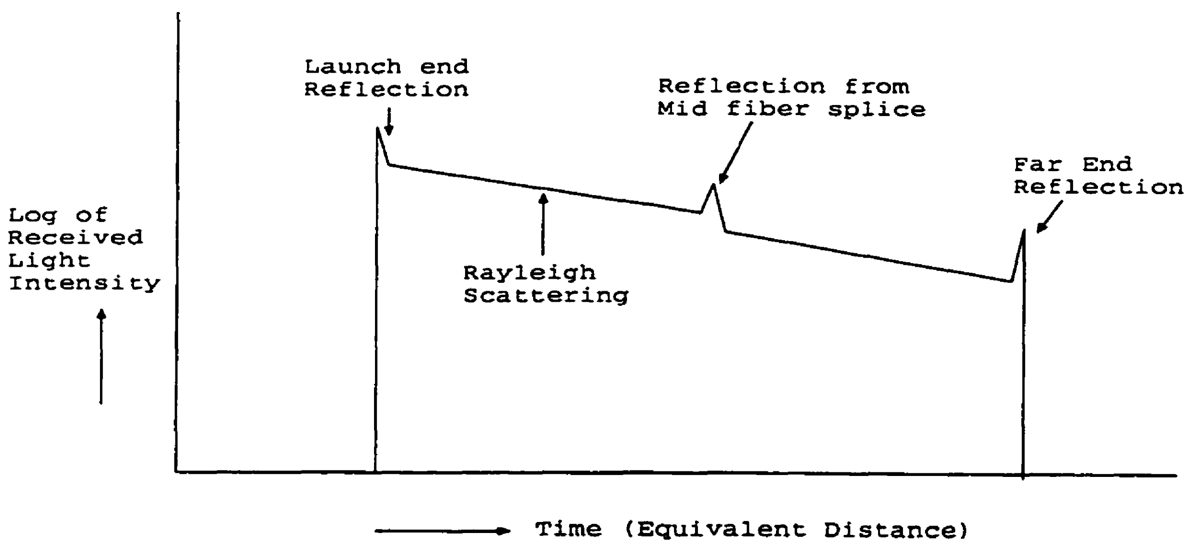

Figure 3.1. OTDR Principle

sensing channel may be backscatter, mode to mode coupling or backscatter through non-linear effects such as Raman and Brillouin scattering.

Optical Time Domain Relectometery (OTDR) (Fig. 3.1) is the most common distributed sensing system used[23] and it utilizes an optical radar concept to measure the backscatter power versus time characteristics when a short pulse of light is launched into the fiber. A special form of OTDR is Polarization Optical Time Domain Reflectometery (POTDR) (Fig. 3.2). In POTDR systems a pulse of polarized light is launched and the detector is arranged to be polarization sensitive by placing a polarizer before it. The method relies on the fact that the Rayleigh and Rayleigh-Gans scattering in silica glass is polarized in the same direction as is the incident light. Any changes in the

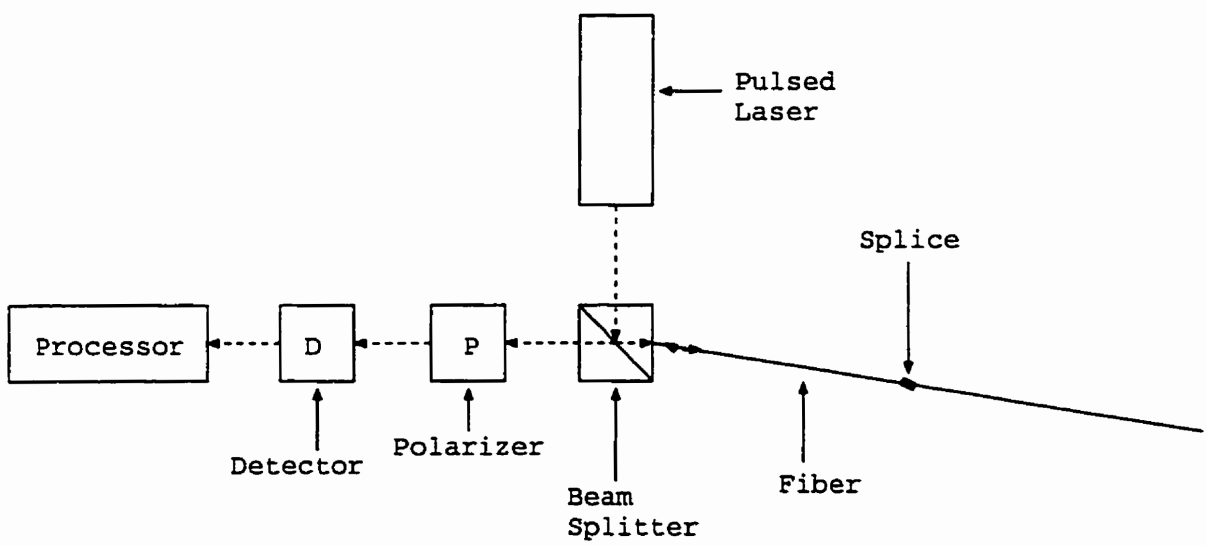

Figure 3.2. POTDR set up

SOP of the detected light result from the changes during propagation over the two-way path to and from the scattering point. Changes in the SOP of light from different points along the fiber result in variation in the detected signal at appropriate delay times.

After comparing all of the above systems in terms of cost, complexity of design, construction time, flexibility etc., it was decided that TDM provided the optimum solution. All the future design considerations were made based on the TDM approach.

3.3 Network Topologies

After having chosen TDM as the multiplexing approach to be used for the network design the next step was to identify the optimum network topology. Three passive topologies were shortlisted for selection :

- Ladder Network
- Ladder Star Network
- Star Network

The criteria for selection were system losses, flexibility, security, ruggedness and of course cost. As the power loss criteria is extremely critical, detailed power loss calculations were made for each topology.

3.3.1 Ladder Network

In the Ladder network of Fig. 3.3 only two main fibers are used; one for transmitting the pulse signals to the input couplers and the other for carrying the modulated pulse signals from the sensors to the receiver. All the sensors in the network are coupled in parallel to these two fibers. The couplers on the transmitting fiber have a tap ratio of 10:90 i.e. 10% of the coupler input power is fed to the sensor. and the couplers on the receiving fiber have a tap ratio of 50:50. The source is a pulsed laser or an LED.

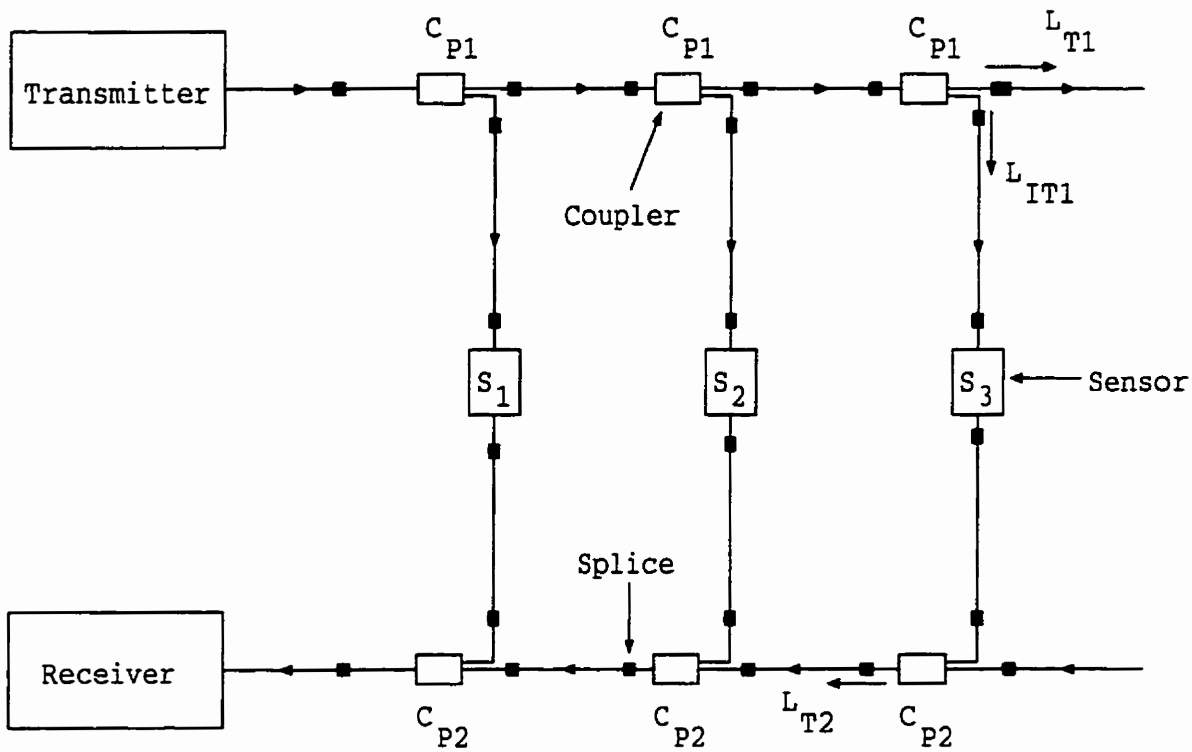

Figure 3.3. Ladder Network

The fact that there are only two fibers makes this system relatively simple but when a large number of couplers and splices are used the losses will become very high. Moreover, there is a slight chance that couplers on the receiving fiber may distort the modulated signals coming from the other sensors and especially if the signals are intensity modulated.

POWER LOSS CALCULATIONS :

N - Number of sensors in the network

C_{P1} - Couplers between the Transmitter and the Sensors

C_{P2} - Couplers between the Sensors and the Receiver

L_{T1} - Tap ratio loss of Coupler on the transmitting fiber (10:90) = 0.46 dB

L_{IT1} - Tap ratio loss of Coupler to Sensor (90:10) = 10 dB

L_{T2} - Tap ratio loss of the Couplers on the receiving fiber (50:50) = 3dB

L_{CI} - Excess loss of each coupler = 0.1 dB

α_s - Splice loss = 0.1 dB

The following relation was derived for the Total System Loss (TSL)

$$TSL = N(L_{T1} + 2L_{CI} + L_{T2} + 4\alpha_s) + L_{IT1} - L_{T1}(dB) \qquad (3.1)$$

Substituting the assumed values for above parameters,

$$TSL = 4.06N + 9.54(dB) \qquad (3.2)$$

As we can see, TSL in the Ladder network increases linearly with the number of sensors in the network.

3.3.2 Ladder Star Network

The design of the transmitting section and the sensor is essentially the same as in the Ladder network with the major difference being in the receiver side. In this system (Fig. 3.4) there is no common fiber between the different sensors and the receiver.

Instead, each sensor is connected individually to the receiver with a separate fiber and via a Star coupler.

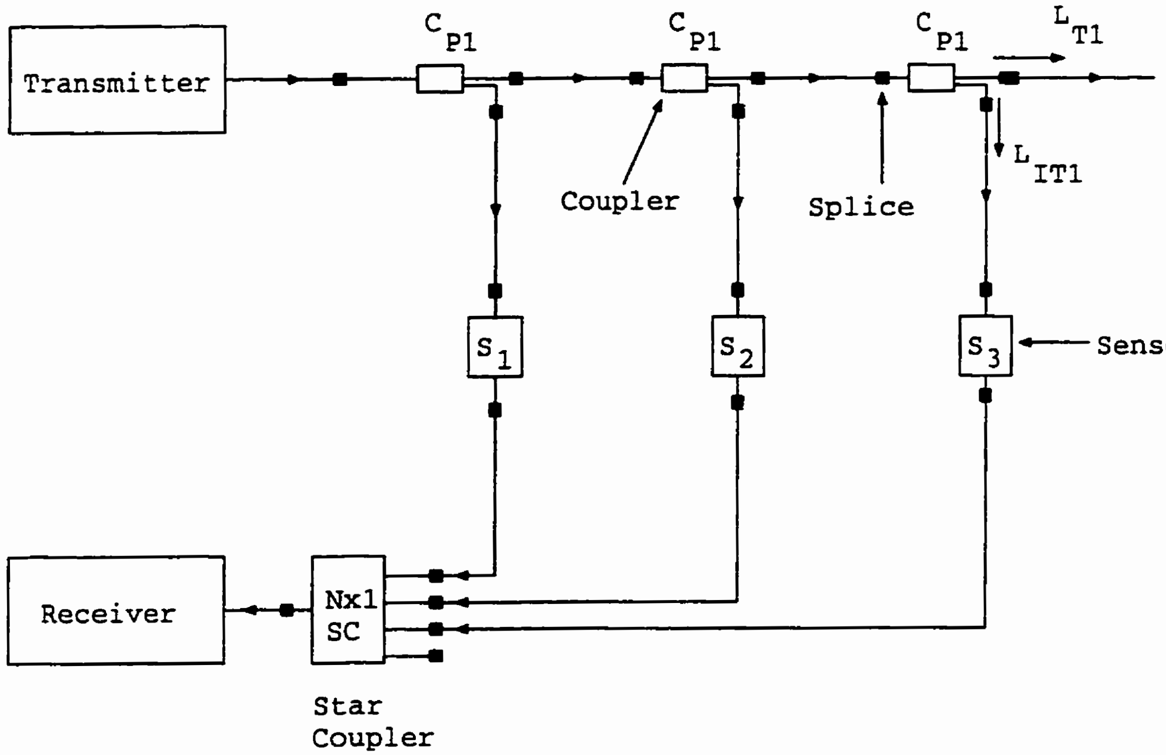

Figure 3.4. Ladder Star Network

With this modification the losses on the receiving fiber, which were a major bottleneck in the previous system, are avoided. However, the issue of security still remains. As there is a common fiber connecting the transmitter to all the sensors, if there is some fault/damage in that fiber then all the remaining sensors will become disfunctional.

POWER LOSS CALCULATIONS :

N - Number of sensors in the network

C_{P1} - Couplers between the Transmitter and the Sensors

L_{T1} - Tap ratio loss of Coupler on the transmitting fiber (10:90) = 0.46 dB

L_{IT1} - Tap ratio loss of Coupler to Sensor (90:10) = 10 dB

L_{CI} - Excess loss of each coupler = 0.1 dB

α_s - Splice loss = 0.1 dB

L_{SC} - Excess loss of Star coupler = 1 to 2.5 dB

L_{TS} - Tap ratio loss of Star coupler = 10 log_{10}N dB

The following relation was derived for the Total System Loss (TSL) :

$$TSL = N(L_{T1} + L_{CI} + 2\alpha_s) + L_{IT1} - L_{T1} + 2\alpha_s + L_{TS} + L_{SC}(dB) \qquad (3.3)$$

Substituting the assumed values for above parameters.

$$TSL = 0.76N + 9.74 + 10log_{10}N + L_{SC}(dB) \qquad (3.4)$$

This system is designed around the TDM technique thus it uses a pulsed source. A continuous beam of light can also be used as the source and it has a number of advantages over the pulsed source. It is easier to find a continuous light source than a pulsed one. it is less expensive. and it also provides more flexibility in positioning and spacing of the sensors which leads to a saving of fiber. The most significant difference in the two systems is the use of an optical switch in place of the Star coupler at the receiving end and this means that the receiver is connected sequentially to each sensor.

The main disadvantage of using an optical space switch is the possible variation in losses at different switch positions and this is highly undesirable, especially in case of intensity modulated sensors. Generally the switching speed is relatively slow and though faster and more accurate switches are becoming available their high costs are prohibitive for this project.

Power losses are the same as in the case of the pulsed source except that now there is no tap loss at the Star coupler and the Star coupler excess loss is replaced by the Switch insertion loss.

$$TSL = 0.74N + 9.74 + L_{SI}(dB) \tag{3.5}$$

where L_{SI} is Switch insertion loss.

3.3.3 Star Network

In this system (Fig. 3.5) one passive star coupler is connected at the transmitter and another at the receiver and each sensor is independently connected to the transmitter and the receiver through these couplers. This system utilizes the TDM technique and therefore a pulsed source is required. The basic design is very robust since each sensor is connected separately thus ruling out any chance of distortion of the signal from another sensor due to the use of a common fiber. Also this system offers a greater level of security than the other systems in the sense that if a fiber is damaged it would not affect the performance of the whole system, and it is very easy to find out which fiber or sensor has been damaged. From the topographical flexibility point of view this system is also extremely good and there are minimal complications involved in adding or removing a sensor.

POWER LOSS CALCULATIONS :

α_s - Splice loss = 0.1 dB

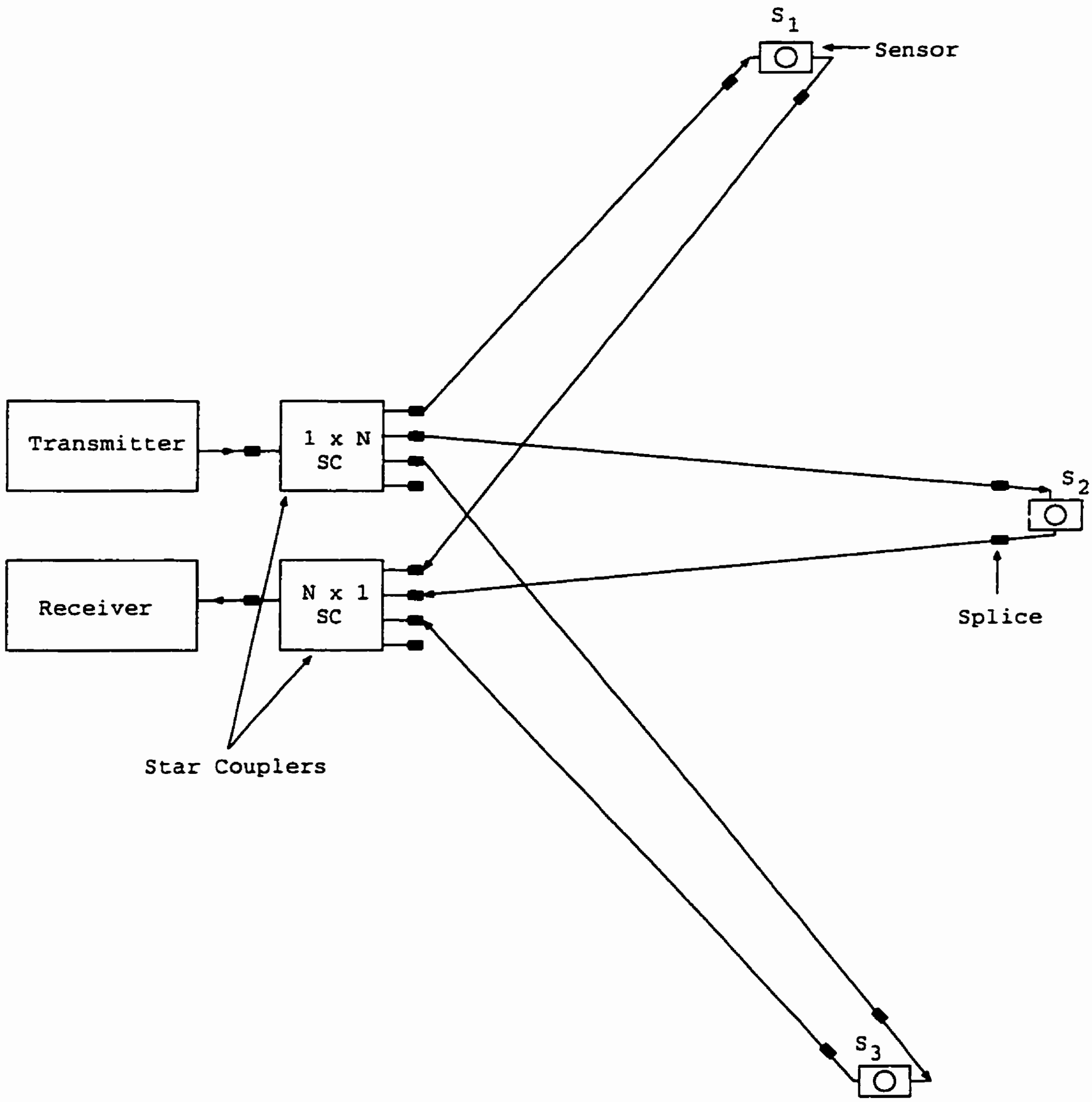

Figure 3.5. Star Network

L_{SC} - Excess loss of Star coupler = 1 to 2.5 dB

L_{TS} - Tap ratio loss of Star coupler = 10 log_{10}N dB

The following relation was derived for the Total System Loss (TSL) :

$$TSL = 2(L_{SC} + L_{TS}) + 4\alpha_s(dB) \tag{3.6}$$

thus :

$$TSL = 2(L_{SC} + 10log_{10}N) + 0.4(dB) \tag{3.7}$$

Here the total system loss is a logarithmic function of the number of sensors in the network rather than a linear function. This means that losses increase very slowly with an increase in the number of sensors in the system.

3.3.4 Comparison of Networks

A comparative analysis was performed for the total system losses of each network topology and how the losses increased with increasing number of the sensors in the network.

From the manufacturer's specifications and data, it has been observed that the excess loss of a Star coupler (1 x 2^n) can be given by L_{SC} = (0.5 x n) dB

It has also been assumed that losses for a 1 x N and an N x 1 Star coupler are the same. Fiber transmission losses are generally not included in TSL calculations.

N	TSL (dB)		
	Ladder	Ladder Star	Star
	$4.06N + 9.54$	$0.76N + 9.74 + 10log_{10}N + L_{SC}$	$2L_{SC} + 20log_{10}N + 0.4$
2	17.66	14.76	7.40
4	25.78	19.78	14.40
8	42.02	26.32	21.40
16	74.50	35.90	28.40
32	139.46	51.56	35.40
64	269.38	79.38	42.40
128	529.22	131.52	49.40

Table 3.1. Comparison of TSL

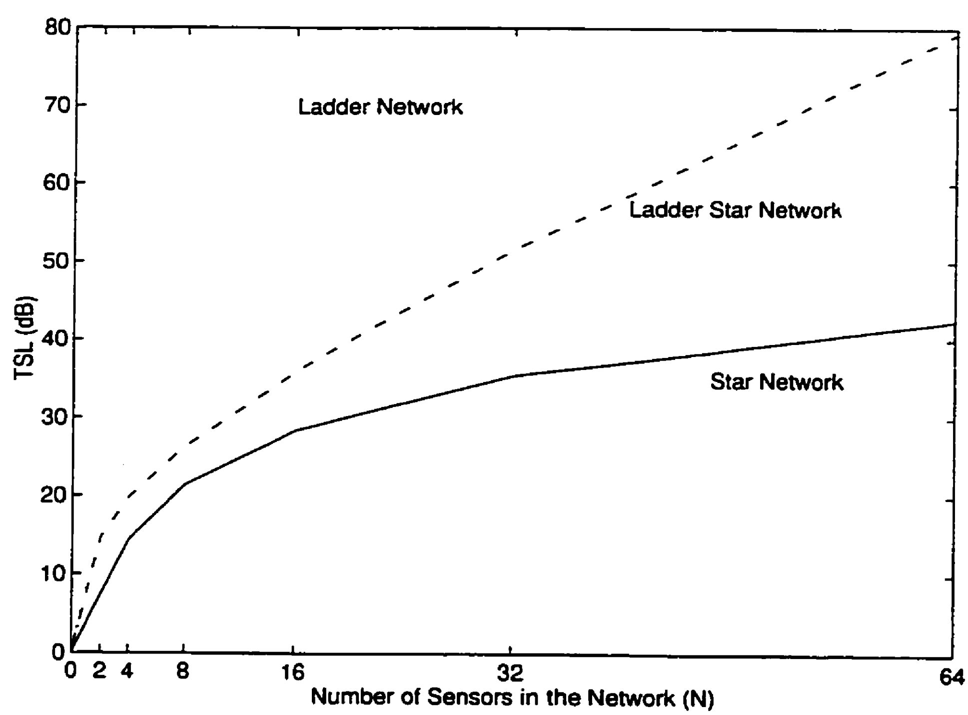

Figure 3.6. Comparison of TSL

It is clear from the the results in Table 3.1 and Fig. 3.6 that the Star network offers the best performance in terms of total system loss and it shows even better results when additional sensors are added to the network. As the Star network promises much smaller system losses and also other advantages like better security, more flexibility, affordability, etc., it was concluded that it was the optimum topology for this project.

3.4 Basic Design of the passive STAR Network

If this project can prove that two fiber optic current sensors can be successfully networked together using a single transceiver unit then the system will also work for any greater number of sensors. As this is a proof of concept project it was decided to use a two sensor network. A very important factor in the actual design of the network is the length of the optical paths between the transmitter and the receiver and especially the difference between the two lengths since the time delay or separation between the two pulses reaching the receiver depends upon this difference. Fig. 3.7 illustrates a timing diagram for the two pulses.

Pulse to sensor 1 = P_{o1}

Pulse to sensor 2 = P_{o2}

Pulse duration = t_p

Time taken by leading edge of P_{o1} to reach Receiver = t_{L1}

Time taken by trailing edge of P_{o1} to reach Receiver = $t_{L1} + t_p$

Time taken by leading edge of P_{o2} to reach Receiver = t_{L2}

Therefore the time separating the two pulses at the receiver is :

$$t_{sep} = t_{L2} - (t_{L1} + t_p) \tag{3.8}$$

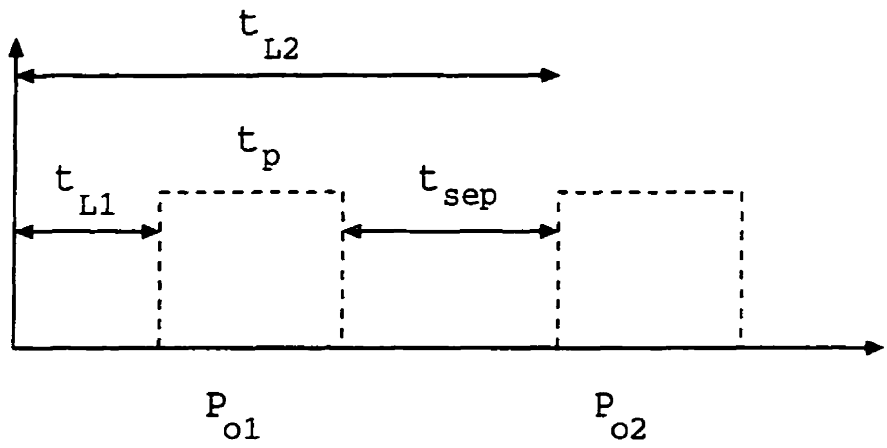

Figure 3.7. Pulse gap at the Receiver

or,

$$(t_{L2} - t_{L1}) = t_{sep} + t_p \tag{3.9}$$

Keeping in mind the requirements of the receiver, the optimal value for both t_p and t_{sep} was found to be 400 ns. It may be noted that a pulse larger than 400 ns can also be used.

Thus,

$(t_{L2} - t_{L1}) = 400 + 400 = 800$ ns

This means that the difference in the two fiber lengths should be equivalent to 800 ns. The actual fiber length difference will now be calculated.

The time taken by a light pulse to travel a distance of L m in a medium having refractive index n is given by $t_L = nL/c$, where c is the velocity of light in free space (3×10^8 m/sec)

For Silicon fiber, $n = 1.5$

Thus :

$L = t_L(2 \text{ x } 10^8)$ m

Therefore to have a time gap of 800 ns between the leading edges of the two pulses the difference in the fiber lengths should be :

$L2 - L1 = (800 \text{ x } 10^{-9})\ (2 \text{ x } 10^8) = 160$ m

So the values chosen for the two fiber lengths were

$L1 = 10$ m, $L2 = 170$ m

The basic design of the two sensor Star network is shown in Fig. 3.8.

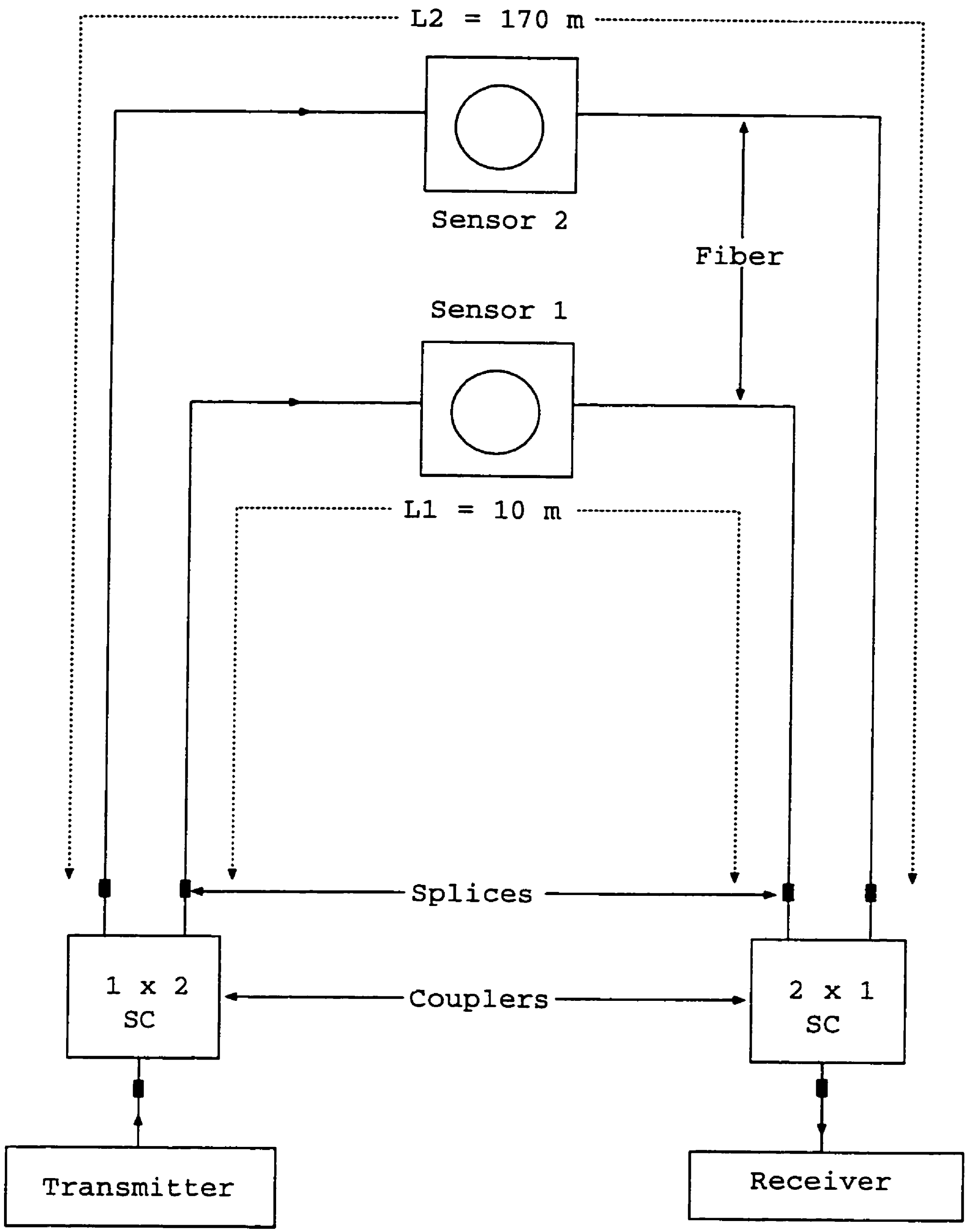

Figure 3.8. Basic STAR Network Design

CHAPTER 4

DESIGN OF THE FOCSNET SYSTEM

4.1 Basic Design

The whole FOCSNET system can be broadly divided into three parts:

- Transmitter
- The Fiber Optic Network and Sensors
- Receiver

The transmitter injects a narrow laser pulse in to the fiber optic network where it is then split into two identical pulses by a star coupler. Each pulse goes to its own current sensor where it undergoes intensity modulation by the sensor. As the two pulses travel different fiber lengths when they appear at the receiver through yet another star coupler they are now slightly modified in amplitude with some time lag between them. This time lag depends on the difference in the lengths of the two fibers. At the receiver the light pulses are converted to voltage signals using a photodiode and operational amplifier and the voltage signal is then processed to give a display of the two electrical current values on a monitor.

4.2 Transmitter

The transmitter consists of a laser diode operating at 820 nm wavelength. The laser diode is modulated by a signal which is generated in the receiver circuit so that the receiver electronics are synchronized with the laser pulses. The laser diode transmits 400 ns wide pulses with intervals of 1.6388 ms between consecutive pulses. The stability of the laser is very important since any change in the value of light pulse will be taken as a change in the current being measured. For this purpose a very highly stable laser source was constructed which had provision for internal thermal compensation and could resist changes in temperature. The laser diode used in it was a SHARP LT017MD and the output from the unit was obtained by way of a pigtailed single mode fiber terminated with an angled connector (FCAPC) and it resulted in a high coupling efficiency from the laser to the fiber.

4.3 Fiber Optic Network

This is the section of the system where the light pulse from the laser diode is split into two identical pulses which are then carried to the two sensors where they get intensity modulated by the current. These intensity modulated signals are then carried back to the receiver section for interrogation. The fiber optic network consists of single mode couplers, variable single mode attenuators, single mode fiber, polarizing fibers and annealed sensing fibers.

4.3.1 Single Mode Couplers

The single mode couplers are used to split the input laser pulse into two pulses and later on to put them together on the same path. The transmit coupler used in this experiment is a 1x2 coupler with an output split ratio of 50:50. A 1x2 optical fiber coupler is essentially the same as a 2x2 coupler except that only one leg is activated at the input. With a 2x2 (50:50) coupler light on any of the two inputs will be split equally in half at the two output fibers.

4.3.2 Variable Attenuators

The light pulses in the two fiber paths may be subject to slightly different optical power losses since losses are not exactly the same for any two similar components. So even when no line current is present in the sensor the intensity levels of these two pulses at the receiver may not be the same. This situation is highly undesirable as it leads to a loss in sensitivity and more complex calibration. To accomodate this situation variable attenuators are used in the network to adjust the intensity levels of the pulses such that when no sensor current is present they both have the same magnitude at the receiver.

4.3.3 Single Mode Fiber

Single mode fiber is used to transmit the input light pulses to the polarizing fiber. Single mode fibers are used since the sensor fibers are also single mode and to get efficient splicing between them it is essential that both have the same core and cladding diameters. Also, by the time the light pulses reach the polarizing fiber, they are depolarized to a very large extent by the SM fiber. Another purpose of these fibers is to provide the required time delay between the two pulses at the receiver and this time separation depends on the relative lengths of the two fibers. In this project the two fiber lengths are 10 m and 170 m which provides a time gap of 800 ns between the two pulses at the receiver.

4.3.4 Current Sensing Head

In the case of the fiber optic current sensor the magnetic field accompanying the current to be measured causes a rotation of the plane of polarization of the light in the sensing fiber and this Faraday rotation has to be optoelectronically measured at the receiver. In the absence of detectors allowing the direct measurement of the polarization direction of light, the relation signal must first be converted into an amplitude signal. This conversion is made in the sensing head which consists of two polarizing fibers (PZ) with an annealed sensing fiber (AF) between them. The annealed sensing fiber is enclosed in a frame which has a circular hole in its middle where the current carrying conductor passes through, with the annealed fiber wound around the hole. The polarization axes of the two polaring fibers are 45° apart[12].

As discussed in Chapter 2 the polarizing fibers in effect act as polarizers. The light coming from the transmitter to the first polarizing fiber through the input coupler and single mode fiber is essentially depolarized in nature. Thus let the light arriving at the input to the first polarizing fiber have intensity J. Also let the intensity of the light coming out of the first polarizing fiber be J_{in} and let J_{out} be the intensity of the light coming out of the second polarizing fiber.

It is well known that the intensity of depolarized light is reduced by half after passing through a polarizer set at any angle[31]. Therefore,

$$J_{in} = \frac{J}{2} \tag{4.1}$$

As discussed in Chapter 2, the intensity of a polarized beam of light passing through another polarizer follows a cos^2 relation of the difference between their polarization axes[16, 31]. If the orientation of the first polarization fiber is assumed to be at θ, then the orientation of the second polarization fiber is at (θ + 45°). When the line current to be measured is zero there is no rotation of the plane of polarization of the light and the intensity of output light can be given by

$$J_{out} = J_{in}.cos^2[(\theta + 45°) - \theta] \tag{4.2}$$

$$= J_{in}.cos^2(45°) \tag{4.3}$$

$$= \frac{J_{in}}{2} \tag{4.4}$$

$$= \frac{J}{4} \tag{4.5}$$

When the line current is present and it rotates the plane of polarization of the light in the sensing fiber by an angle of Ω the difference in the polarization axes of the polarized light and the second polarization fiber is no longer 45° and it becomes (45° - Ω). So now

$$J_{out} = J_{in}.cos^2(45° - \Omega) \tag{4.6}$$

$$= J_{in}.cos^2(45° - \Omega) \tag{4.7}$$

$$= \frac{J_{in}}{2}[1 + cos(90° - 2\Omega)] \tag{4.8}$$

$$= \frac{J_{in}}{2}(1 + sin2\Omega) \tag{4.9}$$

So the change in the intensity can be given as

$$\Delta J_{out} = \frac{J_{in}}{2}(1 + sin2\Omega) - \frac{J_{in}}{2} \tag{4.10}$$

$$= \frac{J_{in}}{2}.sin2\Omega \tag{4.11}$$

$$= \frac{J}{4}.sin2\Omega \tag{4.12}$$

Thus a polarization change is converted to an intensity change which is then detected at the receiver and the corresponding value of the line current is calculated based upon that intensity change. The operation of the current sensor is illustrated in Fig. 4.1.

4.4 Receiver Design

Receiver design is perhaps the single most crucial part of the project and it would not be wrong to call the receiver the heart of the FOCSNET system. Here the intensity modulated optical signals from the sensors are converted to voltage signals and amplified and this signal is then fed to an Analog to Digital Converter (ADC) through a differential amplifier. The differential amplifier is used to bring the voltage signal within the ADC's normal operating input range and also to increase the sensitivity of the system. The ADC which operates at a 20 MHz sample rate digitizes the input signal and then sends the digital output to the Field Programmable Gate Array (FPGA) implemented on a Xilinx chip. The FPGA is designed such that the useful information is extracted and then sent to the Digital Signal Processor (DSP) for processing, which in turn sends the data for display to a Personal Computer (PC) monitor.

4.4.1 Photodiode

The function of the photodiode is like that of a bridge between the fiber optic network and the rest of the receiver electronics. It receives the light signals from the coupler output and converts them to the voltage signals which can be then processed by the receiver electronics.

After careful consideration it was found that HFD-1100 from EG&G was the best

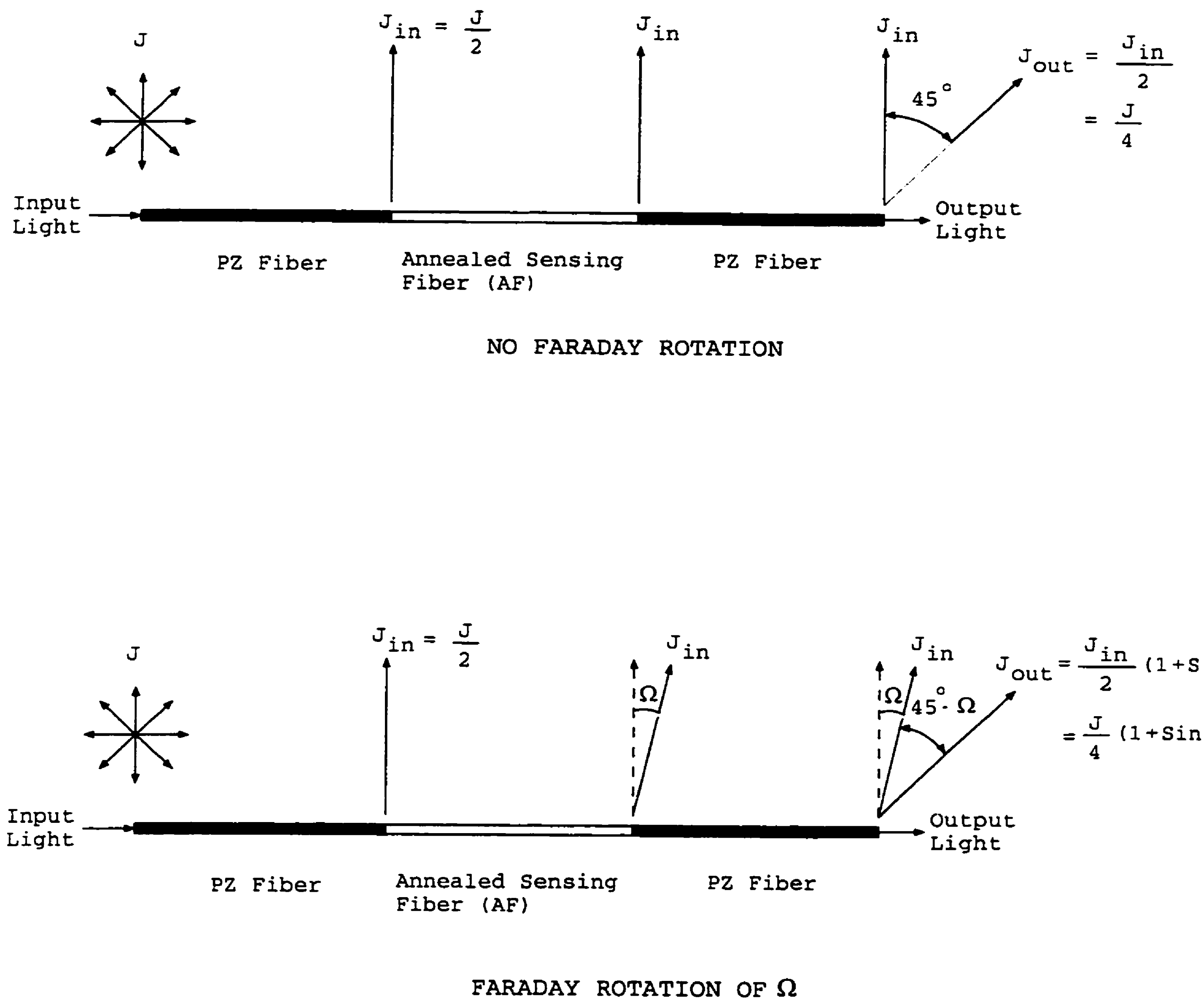

Figure 4.1. Operation of the Current Sensor

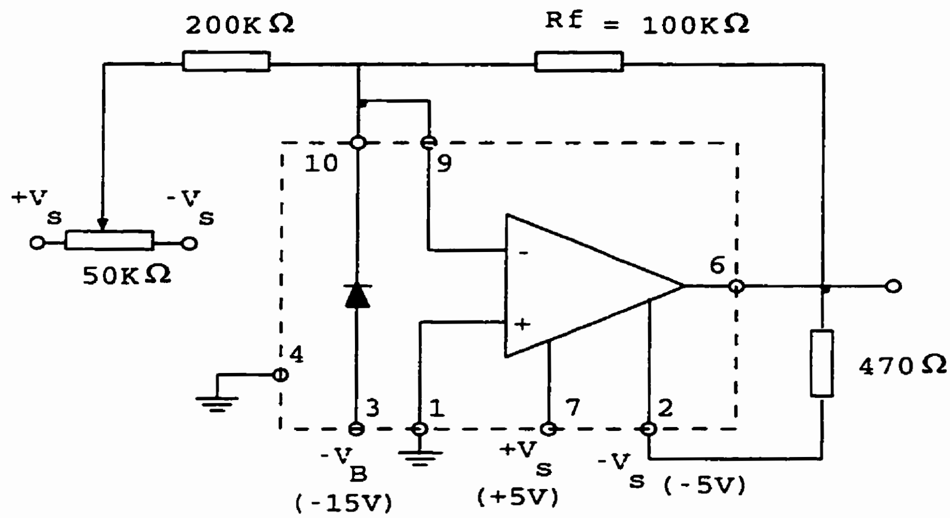

Figure 4.2. Photodiode/Op-amp Circuit Diagram

device for this project since it is an ultra-fast photodiode with a built in operational amplifier. Its main specifications are:

- Responsivity : $6\text{x}10^4$ V/W (850nm)
- System BW(-3dB) : 35 MHz
- Slew Rate : 600 V/μS (850nm)
- Noise Voltage : $7\text{x}10^{-4}$ V RMS
- Spectral Noise Voltage Density : $0.11\text{x}10^{-6}$ $V/Hz^{1/2}$
- Noise Equiv. Power (N.E.P.) : 1.8 $pW/Hz^{1/2}$ (900nm)

The circuit diagram for this photodiode/op-amp is shown in Fig. 4.2. As the pulse width of the light beam is about 400 ns it is essential that the photodiode has very fast rise and fall times. This Photodiode/Op-Amp certainly meets that requirement with a slew rate of 600 V/μs. Moreover its noise performance is also about the best when compared to the other photodiode/Op-Amp combinations commercially available. As it is an integrated combination of photodiode and operational amplifier many inconsistencies and additional noise factors that would have been there, if a stand alone amplifier had been used, are eliminated.

4.4.2 Differential Amplifier

The output voltage signal from the photodiode is fed to a differential amplifier and the use of a differential amplifier serves two purposes. First, it brings the voltage level of the output signal into the optimal operating range of the analog to digital converter which is -1V to +1V and second, it increases the sensitivity of the system by amplifying just the change in the intensity which is the real parameter needed in order to calculate the line current.

The difference signal V_{ref} is provided by a Universal Source (HP 3245A) as it provides highly accurate and very low noise voltage levels. The value of V_{ref} is chosen such that when there is no line current the output of the differential amplifier circuit is zero. Thus the value of V_{ref} is the same as the value of input voltage signal from the photodiode V_{in} when there is no line current. When line current is present it rotates the polarization state of the light which in turn is converted to a change in the light intensity and this change is converted to a voltage signal by the photodiode. Due to the way the differential amplifier circuit is set up only this change is amplified and fed to the analog to digital converter.

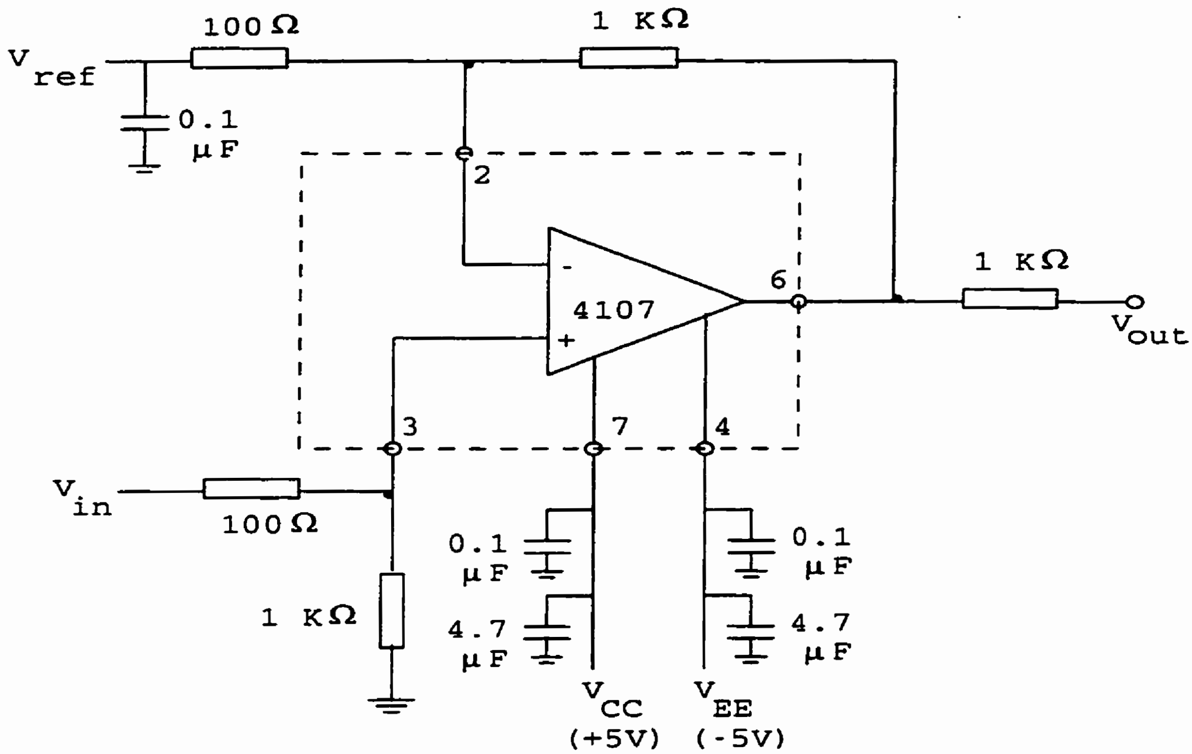

Figure 4.3. Differential Amplifier Circuit Diagram

The choice of the differential amplifier has to be made very carefully since not only should they be very fast and have high bandwidth but they should also have a very low noise performance. After a very careful search the MAX4107 from MAXIM was selected for this purpose and some of its salient features are:

- Bandwidth(-3dB) : 300 MHz
- Slew Rate : 500 V/μS (850nm)
- Settling Time : 18 ns
- Voltage Noise : 0.75 nV/$Hz^{1/2}$

The circuit for the differential amplifier set up is shown in Fig. 4.3 and both the power supplies are connected through two parallel capacitors having capacitances of 0.1 μF and 4.7 μF. The input resistor values used were 100Ω as these were determined to be the optimum values. The manufacturers recommended values were too small since they tended to draw more current from the power supplies thus rendering the amplifier vulnerable to damage by excess current. The feedback resistor has a value of 1KΩ which provides an adequate gain of 10.

4.4.3 Analog to Digital Converter

The A/D Converter digitizes the voltage signal it receives from the differential amplifier and as the system sensitivity depends largely upon the resolution of the ADC then the higher the resolution the greater the sensitivity. The ADC should also be fast enough to fully digitize the first pulse before the second one arrives for sampling. There were three main criteria that were used for the selection of the A/D Converter :

1) Resolution

2) Speed

3) Power Dissipation

The AD9040A is the ADC from Analog Devices which met all of the above criteria. It is a 10-bit 40 MSPS ADC having a Power Dissipation of only 1 watt. Given below are some of its other main characteristics:

- Input Voltage Range : 2 V p-p
- Analog Bandwidth : 48 MHz
- Output Propagation Delay : 14 ns (max)
- SNR at 10 MHz A_{IN} : 53 dB
- Power Supply Rej. Ratio : ± 15 mV/V

This ADC was used along with its evaluation board and it was driven by a 20 MHz clock operating at 50% duty cycle thus it was effectively sampling every 50 ns.

4.4.4 Delay Lines

Delay lines are an important part of the synchronization process between the Xilinx and the actual pulses. To maintain the synchronization the laser diode is modulated by the pulses generated from the Xilinx. This pulse is then split into two pulses which then take predetermined amounts of time to reach the receiver in order to compensate for the different fiber delays. There is more delay in the analog to digital converter before the digital data is ready to be processed by the Xilinx. It is very important that the Xilinx knows just when to fetch the data from the analog to digital converter and this is done by using the Delay lines. These are all-silicon delays which delay the input electrical signal by a fixed amount of time and they are available in 10 tap packages which allows a large choice in delay time values.

Four delay lines were used in this project and all of them were from Data Delay Devices. All of them were 3D7010 having a tap to tap delay of 50 ns and a total delay of 500 ns. Two 3D7010 delays were connected in series giving a total range of

100 ns to 1000 ns. As the two sensor pulses were supposed to have a time lag of 800 ns the outputs from two taps spaced 450 ns apart were connected to the other two delays to obtain further separation.

The leading edge of the modulating pulse from the Xilinx is assumed to be at 0 ns. As the two fiber lengths are 10 m and 170 m the time taken for the leading edges of the two optical pulses to arrive at the receiver is 50 ns and 850 ns respectively. It was found that the analog to digital converter takes 200 ns to sample an input pulse and produce the digital data at its output, thus the total delay required for the leading edges of the two synchronizing pulses is 250 ns and 1050 ns. It is also desirable for pulse stability reasons that the sampling of the pulses be done in the middle of the pulses i.e. at 200 ns point rather than the beginning of the pulses. As the ADC is continuously sampling the data it means that it is the data that appears 200 ns after the leading edge data which is of interest. The Xilinx is then set up to collect the data that appears at a time 450 ns and 1250 ns after the leading edge of the modulating pulse.

The synchronization is performed in the following way. The modulating pulse is input to the first 3D7010 delay and its output tap at 350 ns is connected to the input of the second 3D7010 delay. From this second device two outputs are taken to the inputs of the other two delays. The first output is at the first tap i.e 50 ns and the second output at the last tap at 500 ns hence the total delays are 400 ns and 850 ns. To increase the delays to 450 ns and 1250 ns the outputs from the next delays are taken from the first tap i.e 50 ns and the eighth tap i.e. 400 ns. respectively. Now the total delays are respectively 450 ns and 1250 ns, which are the exact values required by the Xilinx. As soon as the Xilinx receives the leading edge of each of these synchronizing pulses it collects the binary data available at the ADC output and processes it thus ensuring that the data collected by the Xilinx is the digitized form of the analog value taken at the middle of the optical pulses.

4.4.5 Xilinx

If the receiver can be said to be the heart of the FOCSNET system then the Xilinx can be thought of as the brain of the receiver and it is absolutely essential that the Xilinx design work exactly as it is supposed to. This is due to the nature of the data it is collecting which is available for only 50 ns and even a little bit of mis-synchronization can ruin the whole system. The device selected for implementing the FPGA design was the Xilinx XC4003A chip and the design was done using the 'Workview Plus' software on a PC.

The two most important functions of the Xilinx design are to generate the modulating pulse and to fetch the digitized data from the ADC and send it to the Digital Signal Processor.

First the design of the pulse generator (Fig. 4.4). A 20 MHz clock pulse (CIN) is supplied to the Xilinx by a Raltron Crystal in the form of a clock signal to a 4 bit binary counter CB4CE whose Clock Enable (CE) is always kept high and Clear (CLR) always kept low. The third bit of the counter is taken as the output producing a 2.5 MHz pulse which is given as the clock signal to a 16 bit counter CB16CE through an inverter. The inverter is used so that this pulse is initially in the 'high' logic state.

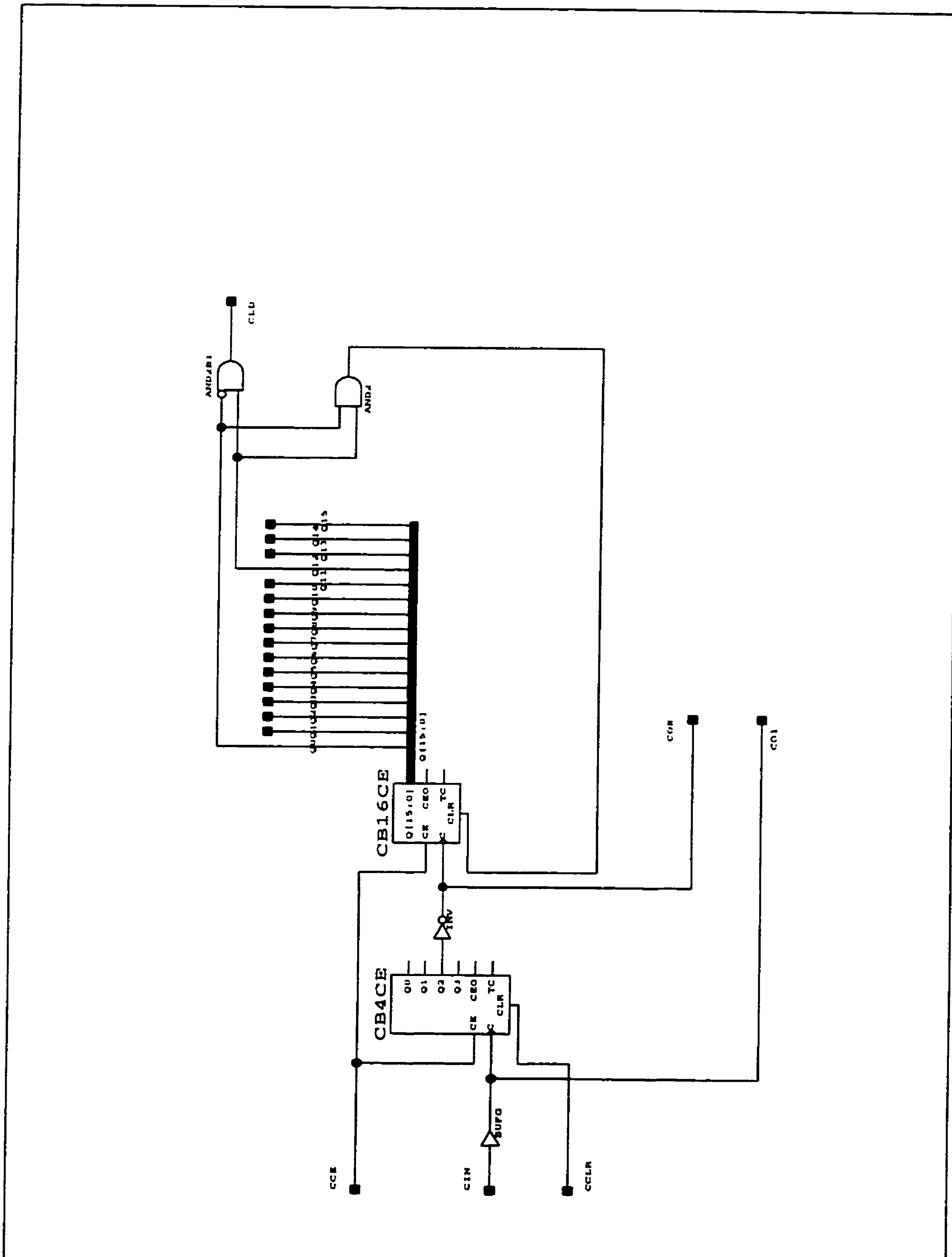

Figure 4.4. Pulse Generator Circuit Design

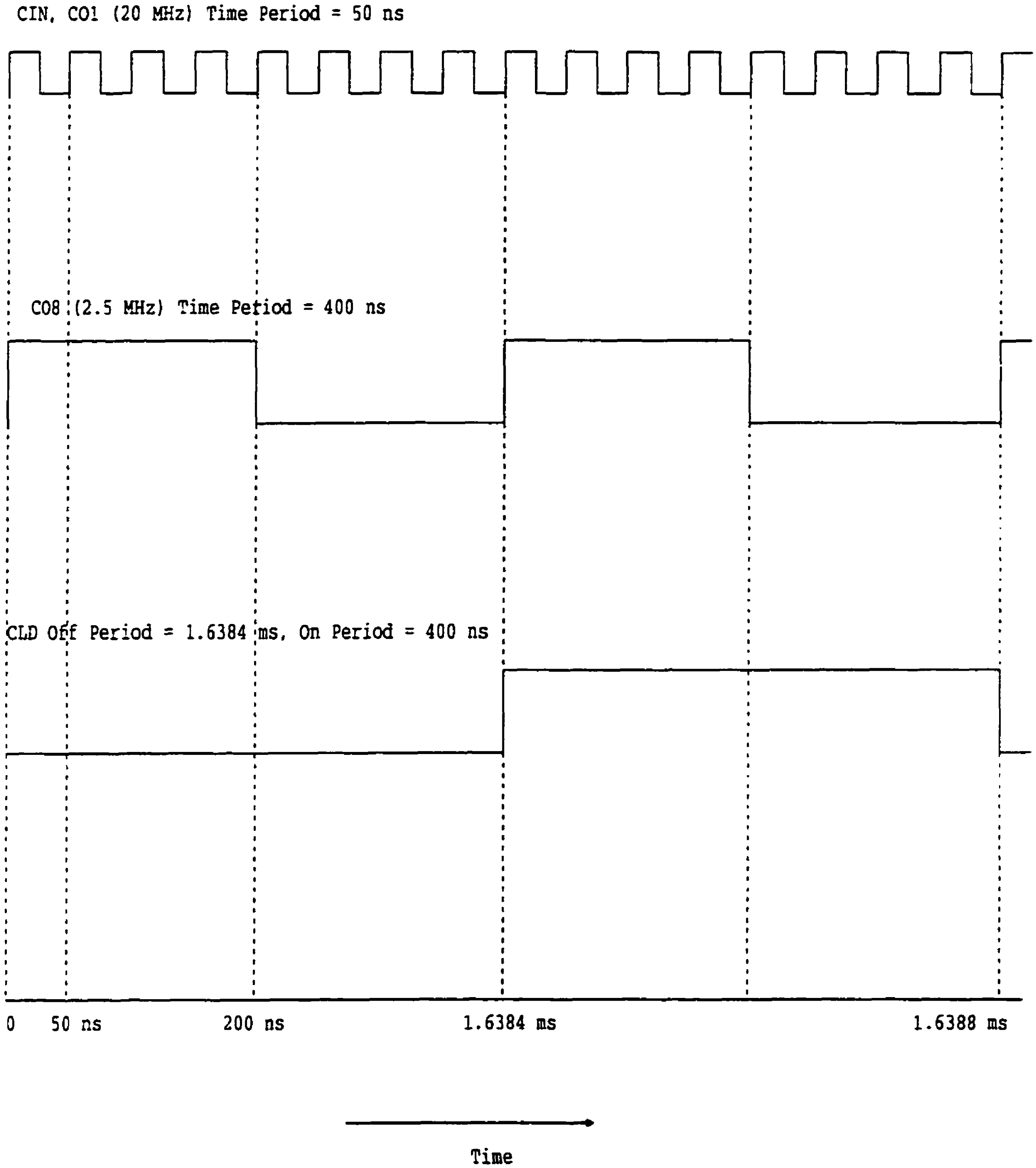

Figure 4.5. Timing Diagram of the Generated Pulses

The output from this counter is taken in such a way that when bit 0 is low and bit 12 high i.e. after 4096 clock pulses, the output is in the high logic state. This lasts for only one clock cycle because when the next pulse comes the bit 0 becomes high and the combination sends a high signal to the Clear (CLR) of this counter and it is reset to zero again and the whole process goes on repeating. As the clock pulse to the 16 bit counter has a time period of 400 ns therefore the output pulse is 'on' for 400 ns and it is repeated every 4097 cycles i.e. 1.6388 ms. This pulse is used both for modulating the laser diode as well as the input to the delay lines and the timing diagrams for this circuit are shown in Fig. 4.5. The 20 MHz clock pulse (CIN) from the crystal is forwarded as clock pulse CO1 to drive the ADC board.

The second important function of the Xilinx design is to act as an interface between the Analog to Digital Converter and the Digital Signal Processor but it first has to get the data from the ADC output. As the two synchronizing pulses are separated by just 800 ns coming to the Xilinx with the next set coming relatively slowly after 1.6388 ms. it was concluded that these two pulses should be held in different locations in order that the DSP have lots of time available to pick them up. This was done using three sets of 11 flip-flops in the Separator circuit (SEPARATOR) which is shown in Fig. 4.6.

The two pulses from the delay lines L1 and L2 (Fig. 4.7) are combined using an OR gate and this signal is sent as DCLK to the SEPARATOR. On each rising edge of the DCLK pulse the set of flip-flops (FDC) latch the data available at the ADC output which is connected to the Xilinx as A0 - A9 and appears to the SEPARATOR as D0 - D9. For this input set of flip-flops there are two output sets of flip-flops,

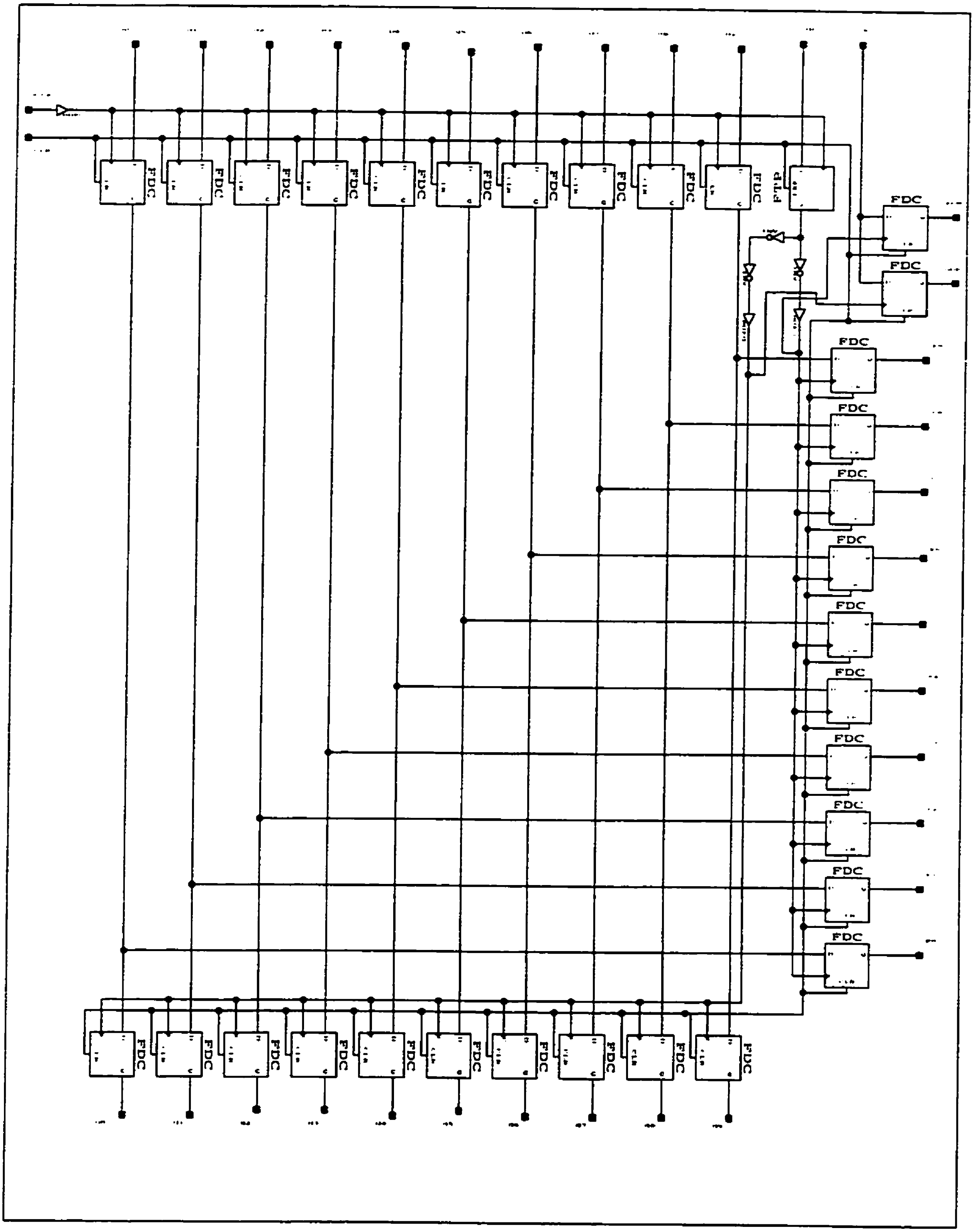

Figure 4.6. The SEPARATOR circuit

F0 - F9 and G0 - G9. The input set of data is available to both the output sets of flip-flops but only one latches to the data while the other one latches the next set of data and this cycle continuously repeats itself. This process is controlled by a toggle flip-flop (FTP) which is driven by DCLK as its clock pulse. The way the toggle flip-flop works is that its output changes state after each clock pulse, hence the name toggle flip-flop and its output goes straight to one set of output flip-flops as their clock while it goes to the other set through an inverter. This insures that only one set is active at a time and they get data on alternate DCLK pulses.

When the first DCLK pulse arrives (due to L1), the input set latches the values D0 - D9 and they are available at their output until the next DCLK pulse arrives. The way the toggle flip-flop is connected to the output sets of flip-flops is that for the first DCLK pulse its output is low and therefore the clock to the set F0 - F9 goes high. So this set latches the output available from the input set which then appears at their outputs. Similarily for the second DCLK pulse (due to L2) the data appears at the output of the second set G0 - G9. The next set of DCLK pulses will arrive after 1.6388 ms.

Now that both the data values are available on different outputs it will be explained how the Xilinx communicates with the DSP and sends these values to it. The overall Xilinx design is shown in Fig. 4.7. The output sets from the SEPARATOR circuit are available on output ports O0 -O9 which are connected to the DSP through multiplexer switches as shown in the diagram. All these switches are controlled by the Data Selector pin (DS) which is also connected to the DSP so that the DSP controls which data set it is reading. But how does the DSP know when a new set of data has

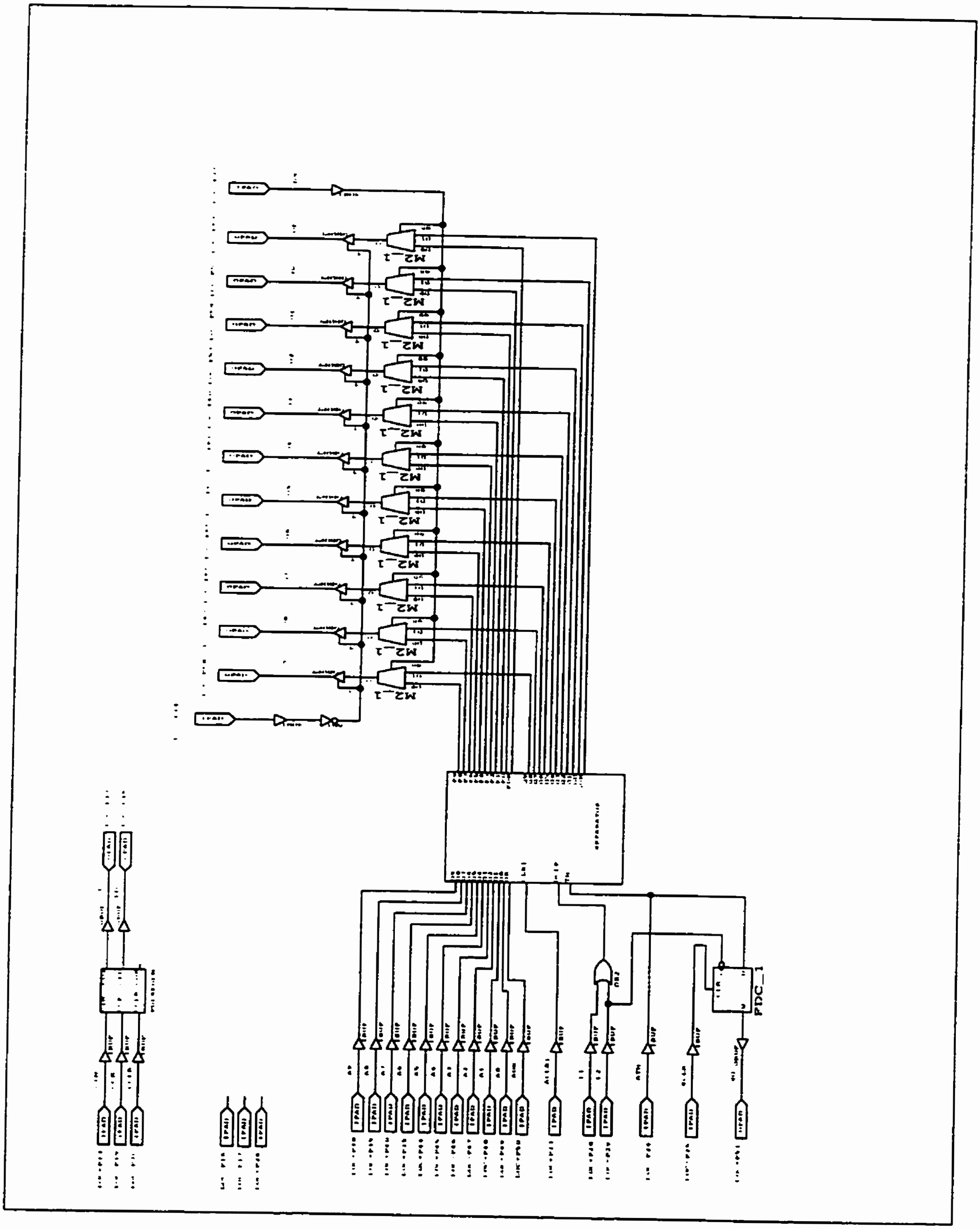

Figure 4.7. The Xilinx Design

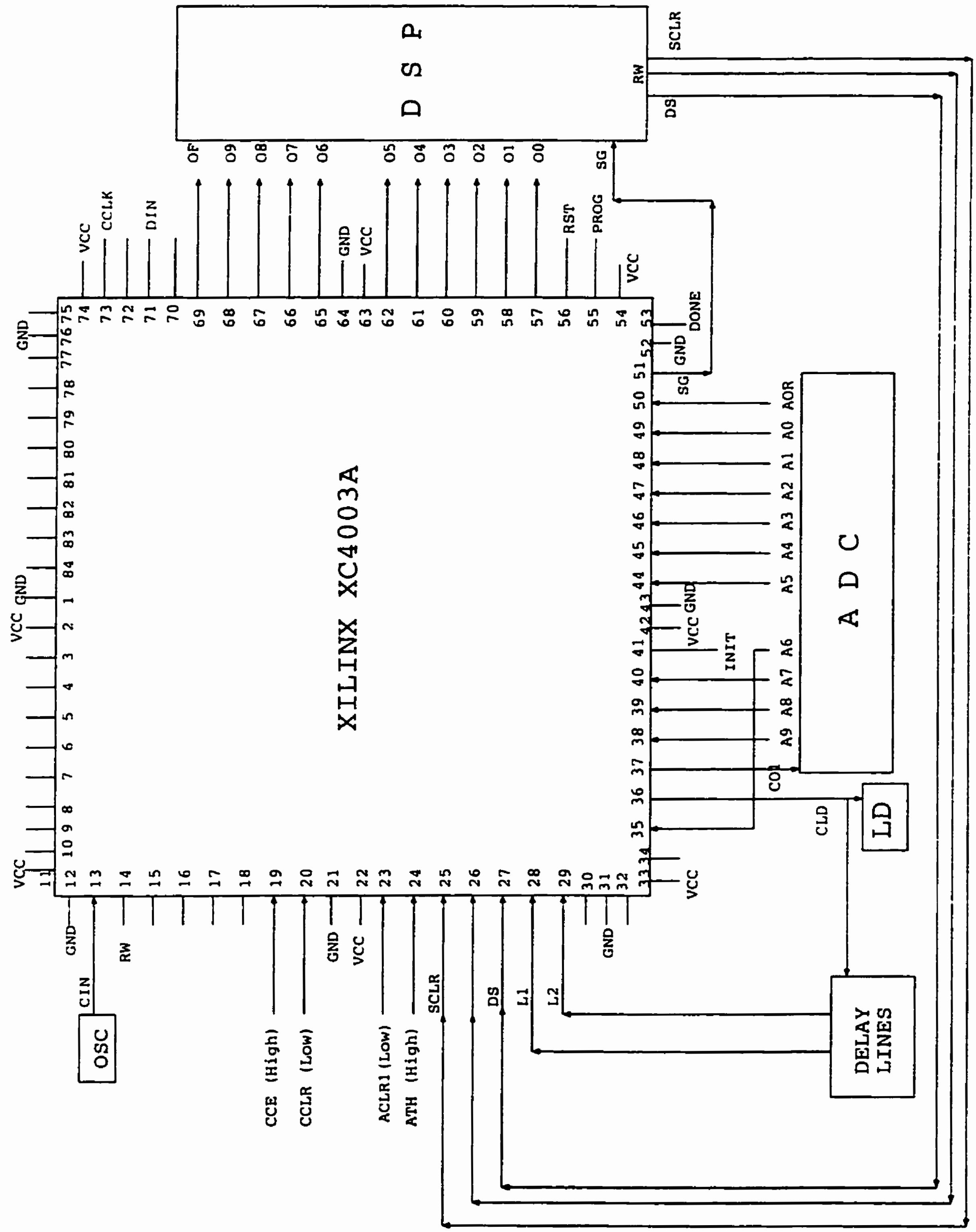

Figure 4.8. The Xilinx Pin-out Diagram

arrived so that it can read the values? This problem is solved by using a flip-flop whose output and clear pins are connected to the DSP. When the falling edge of the second pulse L2 arrives the output of the flip-flop (SG) goes high indicating that the new set of data is ready and that the DSP should read their values. Thus the DSP reads the first set of data when the value on the DS pin is 0 and it then changes the DS pin value to 1 to read the second set of data. After it has read both sets of values it gives a high signal to the clear pin (SCLR) of the flip-flop and therefore resets its value to low state.

This is the way the Xilinx interacts with the DSP and transfers the data contents it receives from the ADC to the DSP where further processing takes place. The Xilinx pin out diagram is shown in Fig. 4.8. The pins INIT, DONE PROG, DIN and CCLK are used to download the bitstream file from the PC to the Xilinx chip.

4.4.6 Digital Signal Processor

As the Xilinx sends each reading at 1.6388 ms intervals it is not possible to observe values changing at such a fast rate. Some mechanism is therefore required to display the readings at a slower rate which are easy to read and at the same time be able to detect and show changes quickly and this is where the digital signal processor comes into the picture.

The following is a summary of the DSP operation:

1) Initially the two accumulators and the counter are set to zero.

2) The DSP checks if the SG signal is high or not.

3) If the SG signal is high then it sends its data bus to fetch the first data value.

4) It stores the value in a memory location, increments the pointer so that next value is stored in the next location and also adds this value to the first accumulator.

5) It changes the value on the DS signal to logic '1' in order to read the second data value and it then reads the second value.

6) Once again it stores the value, increments the pointer and adds it to the second accumulator.

7) Increments the Counter by 1 and checks to see if it is 1024.

8) If it has added 1024 values it divides the value of the accumulators by 1024 thus averaging each of the two values. It then sends the averaged values to the PC for display and also resets the accumulators and the counter to zero.

9) After completing the whole process it sends a high SCLR pulse thus setting the SG signal to the low state and it goes into a loop waiting for the SG signal to go high again.

It can be seen that the DSP utilizes its high speed to get the data from the Xilinx quickly, do all the operations on it and then send the averaged values to the PC for display. The DSP used for this project was TMS320C31 from Texas Instruments. It has a 40 ns instruction cycle time, 50 MFLOPS and 25 MIPS speed. This DSP was used along with its application development board called the DSP Starter Kit (DSK). This board was very helpful as it provided the freedom to create custom software on a host PC, download the software to DSK and run and test the software on the DSK board. The supplied debugger is Windows oriented thus simplifying the code development and debugging capabilities.

4.4.7 Personal Computer (PC)

The DSP sends the averaged values to the PC every 1.6388 ms for display and this means that the speed of the PC is very important therefore a Pentium based 133 MHz PC was used. There is another very significant advantage of using the PC for displaying the results. The values can be easily shown in any desired format and if a formula has been worked out for the calibration of the voltage signals in terms of the measured line current it is very easy to do these little modifications in the PC only, without disturbing the rest of the system, and to show on the PC the value of line current being measured.

A functional diagram of the entire receiver is shown in Fig. 4.9.

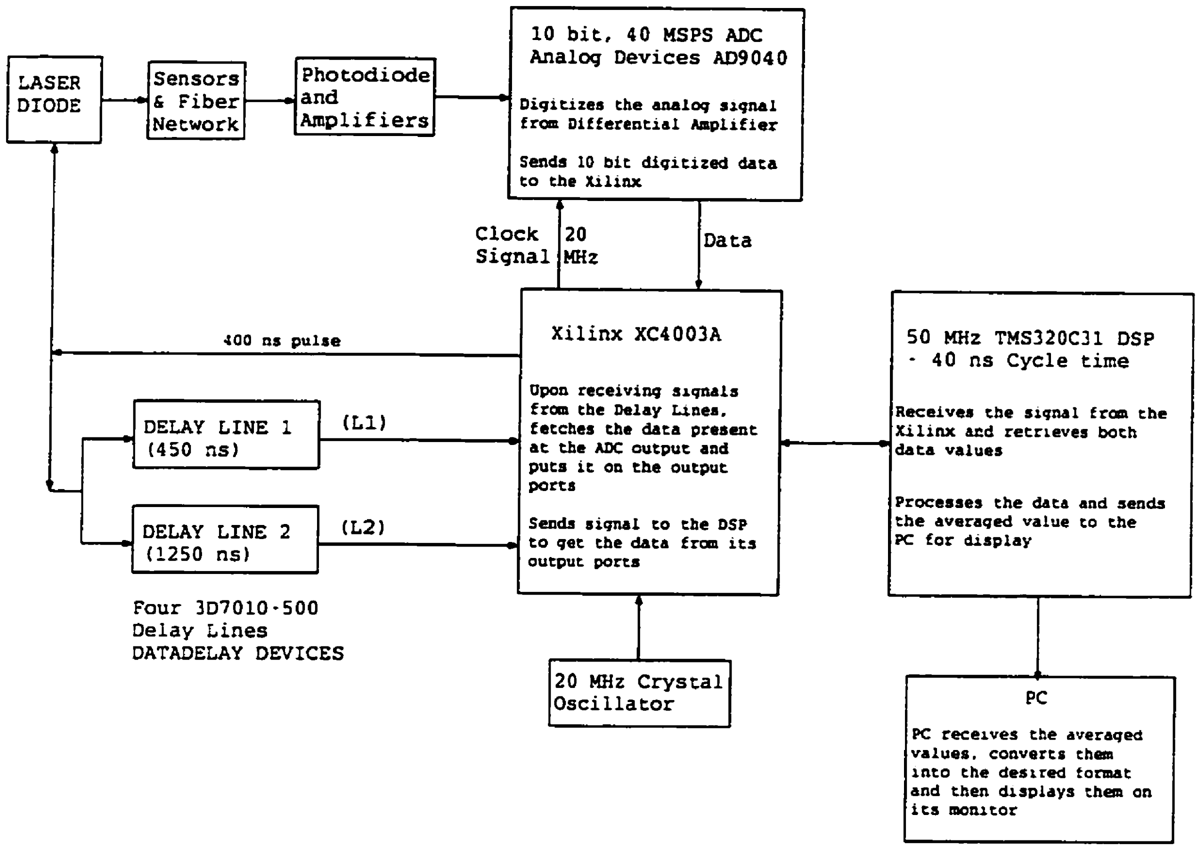

Figure 4.9. Receiver Functional Diagram

CHAPTER 5

PREDICTED PERFORMANCE

5.1 Faraday Rotation

As discussed in Chapter 2 the Faraday rotation angle is highly dependent upon the Verdet constant of the fiber. The higher the Verdet constant of the fiber, the larger is the Faraday rotation resulting in a larger intensity change. Even though the Verdet constant of the annealed sensing fiber is not large, the Faraday rotation angle can be effectively made larger by increasing the number of turns of the current carrying cable around the current sensor.

The Verdet constant of the annealed sensing fiber is around 0.01 min/A at a wavelength of 820 nm[16, 46]. This value is approximate as the annealing of the fiber may have resulted in some variations and it may also differ for different annealed fibers even though manufactured by the same company.

The value of Faraday rotation Ω is calculated as follows. The annealed sensing fiber is wound 4 times around the conductor and the current carrying conductor is wrapped 14 times around the sensor unit. Therefore the Faraday rotation angle is

$$\Omega = VNI$$

or,

$$\Omega = \left(\frac{0.01}{60}\right)(4)(14)(1)\ degrees/A = 0.00933^{\circ}/A$$

For 100 A of D.C. current which is the maximum that could be obtained the Faraday rotation angle will be 0.933°. Fig. 5.1 shows the theoretical linear relationship between the current through the conductor wrapped 14 times around the sensor and the Faraday rotation angle.

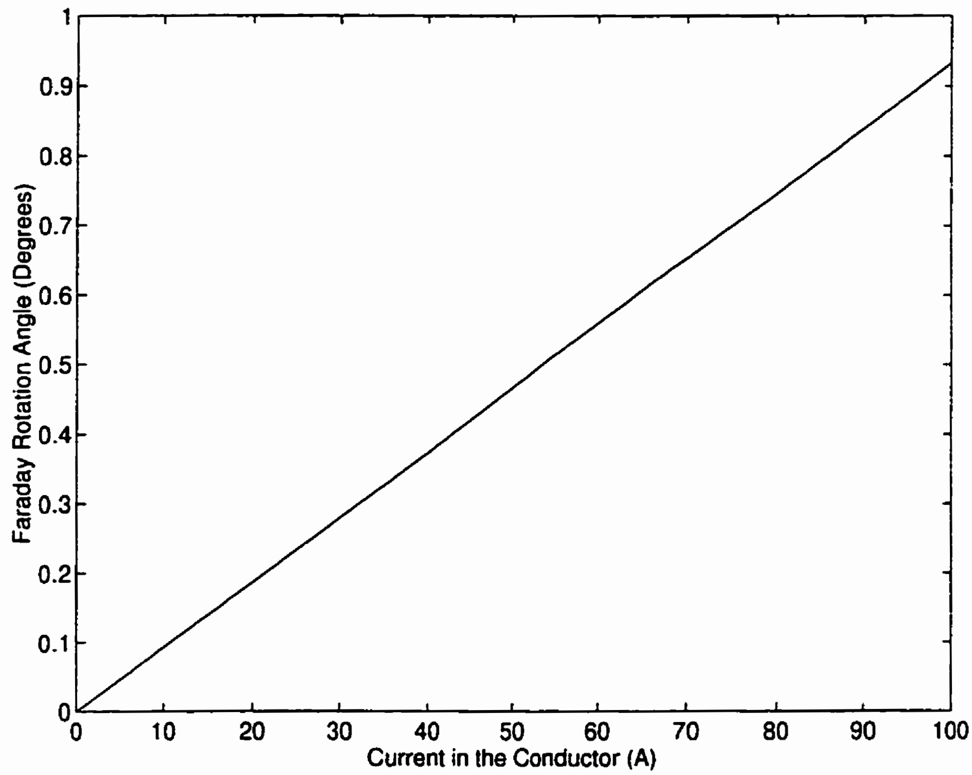

Figure 5.1. Faraday Rotation Angle in the Current Sensor

5.2 Optical Power Loss

As the relative change in the output intensity of light being received by the photodiode is quite small, it is necessary to have a large received intensity of light so that although the relative change is the same the net change is more thus making it easier to measure the change in the intensity of light and determine the Faraday rotation.

5.2.1 Input Coupler Loss

At the input coupler the light is split into two halves of equal intensity with each one going to a different sensor resulting in a 50% loss. The total insertion loss for a 2 x 2 coupler is approximately 3.5 dB.

5.2.2 Fiber Loss

As the light travels through a fiber it experiences some attenuation over the length of the fiber. For the 3M single mode fiber being used in this project the attenuation is 2.1 dB/km. In the FOCSNET the fiber lengths used are 10 m and 170m thus the fiber attenuation for the longer path is around 0.36 dB.

5.2.3 Current Sensor Loss

As explained in the working of the current sensor in Chapter 4 the light suffers a loss of 75% or 6 dB while passing through the current sensor. This is due to the relative orientation of the two polarizing fibers which being at 45° to each other results in a 3 dB loss and there is also a 3 dB loss when unpolarized light goes through the first polarizing fiber.

5.2.4 Output Coupler Loss

At the output coupler the light from the two current sensors is combined and the output goes to the receiver through a single fiber pigtail. However only 50% of the light from each input channel is sent to the output channel as basically there are two output channels but only one is used. So the tap loss here is 50% and the insertion loss is also approximately 3.5 dB.

5.2.5 Connector and Splice Loss

In the whole network both the optical paths consist of three mechanical splices and two FC connector adaptors. Each connector has an insertion loss of about 0.2 dB and each mechanical splice an insertion loss of about 1 dB. Thus the total insertion loss for all the connectors and splices in the network is approximately 3.4 dB.

5.2.6 Other Losses

The other losses include the attenuations due to imperfectly cleaved or slightly unclean fiber ends, bending of the optical fiber etc. These losses are estimated at 2 dB.

5.2.7 Total System Optical Power Loss

The total system optical power loss is the summation of all the above mentioned losses which comes out to be 18.76 dB or 98.67%. The attenuation factor of the system is

$$\alpha = 10^{(-18.76dB/10)} = 0.0133 \tag{5.1}$$

Thus only around 1.33% of the light transmitted by the laser pigtail makes its way to the photodiode.

Sources for the Optical Loss	**Estimated Loss (dB)**
Input Coupler Loss	3.5 dB
Fiber Loss	0.36 dB
Current Sensor Loss	6 dB
Output Coupler Loss	3.5 dB
Connector and Splice Loss	3.4 dB
Other Losses	2 dB
Total System Optical Power Losses	**18.76 dB**

Table 5.1. Optical Power Losses in the FOCSNET

5.3 System Signal to Noise Ratio

The system signal to noise ratio (SNR) is one of the most important parameters for the evaluation of the measurement quality. An electric current is the contribution of many individual electron movements and each electron moves in a stochastic manner[15]. Because of the quantum nature of the electric current each electronic component is more or less a noise source in the circuit.

The electronic components in the FOCSNET system are in the receiver and the main contributor to the system noise is the photodiode/op-amp. The photodetection unit is basically a trans-impedance amplifier which converts the photocurrent into a voltage signal. The noise in this circuit belongs to two categories, the shot noise of the photodiode and the thermal noise of the resistors.

5.3.1 Shot Noise

Shot noise is generated by current flowing through the device. This current consists of both the dark current and the photocurrent. The shot noise current can be calculated by the formula[15, 47]:

$$I_s = \sqrt{2e(I_d + I_p)\Delta f} \tag{5.2}$$

where,

e = Electronic charge (1.6 x 10^{-19} C)

I_d = Dark current (A)

I_p = Photo current (A)

Δf = Noise equivalent bandwidth (Hz)

The equivalent noise voltage at the output V_s is

$$V_s = R_f.I_s \tag{5.3}$$

where R_f is the feedback resistor.

5.3.2 Thermal Noise

The thermal noise is caused by the three dimensional random thermal movement of free electrons in the resistor[15, 47]. The thermal noise current is equal to:

$$I_t = \sqrt{\frac{4kT\Delta f}{R_f}} \tag{5.4}$$

where,

k = Boltzmann's constant (1.38 x 10^{-23} J/K)

T = Temperature (K)

Δf = Noise equivalent bandwidth (Hz)

R_f = Feedback resistance (Ohms)

The equivalent noise voltage at the output V_t is

$$V_t = R_f.I_t = \sqrt{4kT\Delta f R_f} \tag{5.5}$$

5.3.3 Op-amp Noise

The op-amp noise is generally specified by the manufacturer of the device. The amplifier noise can be given as[15, 47]:

$$I_{amp} = \sqrt{\left[I_n^2 + \left(\frac{V_n}{R_{in}}\right)^2\right]\Delta f} \tag{5.6}$$

where,

I_n = Op-amp input noise current ($A/\sqrt{Hz}$)

V_n = Op-amp input noise voltage ($V/\sqrt{Hz}$)

R_{in} = Op-amp input resistance (Ohms)

Δf = Noise equivalent bandwidth (Hz)

The equivalent noise voltage at the output V_s is

$$V_{amp} = R_f . I_{amp} \tag{5.7}$$

where R_f is the feedback resistor.

5.3.4 Total System Noise

Total system noise can be given by:

$$V_{noise} = \sqrt{V_s^2 + V_t^2 + V_{amp}^2)} \;\; V(rms) \tag{5.8}$$

where V_{noise} is the total system noise voltage at the output.

According to the manufacturer's specifications[48], the total noise for photodiode/op-amp HFD-1100 V_{noise} = 700 μV (rms).

5.3.5 Signal to Noise Ratio

The output voltage signal from the photodiode/op-amp is expected to be about 1 V maximum. Therefore the intensity change signal due to Faraday rotation is

$$V_{signal} = 1. \, sin\, 2\Omega \tag{5.9}$$

where Ω is the Faraday rotation angle.

As shown earlier, the Faraday rotation angle for a 100 A D.C current is 0.933° thus the signal voltage for this current is

$$V_{signal} = 1 \text{ x } \sin(2 \text{ x } 0.933^\circ) = 1 \text{ x } 0.0326 = 0.0326 \text{ V}$$

Therefore, for a 100 A of D.C. current the signal to noise ratio SNR of the system is

$$SNR = 20\ log_{10}\left(\frac{V_{signal}}{V_{noise}}\right)\ (dB) \tag{5.10}$$

or,

$$SNR = 20\ log_{10}\left(\frac{0.0326}{(700)(10^{-6})}\right) = 33.36\ (dB)$$

5.4 System Resolution

The system resolution or the minimum detectable current is the current at which the signal to noise ratio drops to 1 or $V_{signal} = V_{noise}$. So the minimum detectable Faraday rotation angle Ω_{min} is

$$(700)(10^{-6}) = 1.\ sin\ 2\Omega_{min}$$

or,

$$\Omega_{min} = 0.02^\circ$$

The minimum detectable current I_{min} is

$$I_{min} = \frac{\Omega_{min}}{0.00933} = 2.14\ A$$

Thus the minimum detectable current, with 14 conductor turns, is 2.14 A.

CHAPTER 6

EXPERIMENTAL INVESTIGATIONS AND RESULTS

6.1 Fiber Optic Current Sensor Networking System

Fig. 6.1 shows the basic components of the FOCSNET system. In this proof-of-concept system a Laser diode transmitter is used to provide the light pulses at 820 nm wavelength. The current sensing head makes use of the frame structure where the light encircles the power line and thus the integral equation, $\Omega = V \oint \vec{H}.d\vec{l} = V.I$ is satisfied. The effects of magnetic fields generated by other power lines located outside of the current sensor frame are theoretically eliminated. In order to simulate large current sensing the power line is twined N times around the frame of the sensor thus effectively increasing the current enclosed by the sensor head by N times. The current sensor is shown in Fig. 6.2

As explained in Chapter 4 the presence of the current in the power line induces a Faraday rotation in the sensing fiber which is converted to an intensity change and this intensity change is detected and measured by the receiver . The difference in the optical paths of the two sensors allows the pulses arriving at the receiver end to be separated in time and thus processed individually.

6.2 Laser Characteristics

The FOCSNET system assumes that the Laser output intensity is constant. As the stability of the laser is highly important, and any changes in its output will be

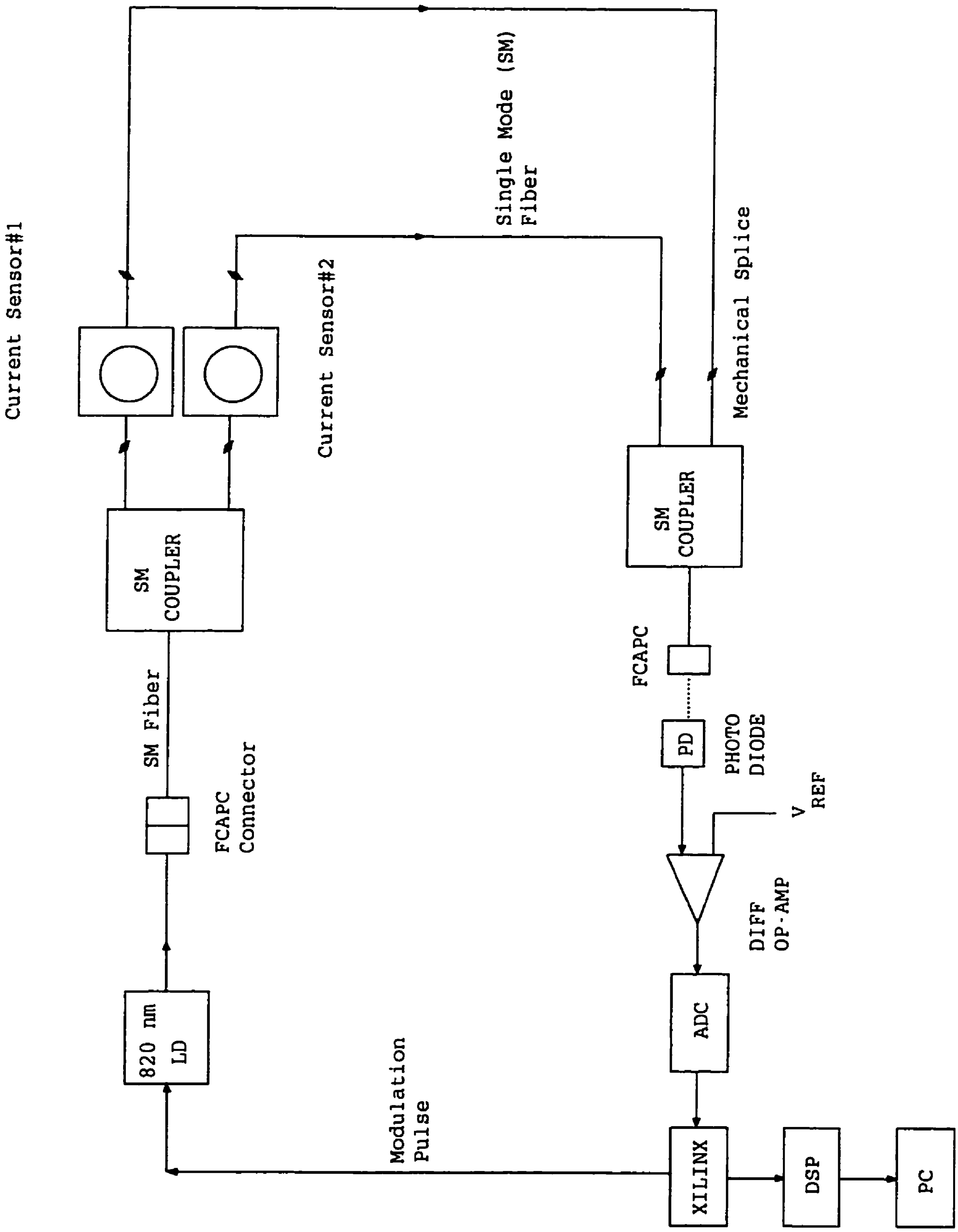

Figure 6.1. Fiber Optic Current Sensor Network

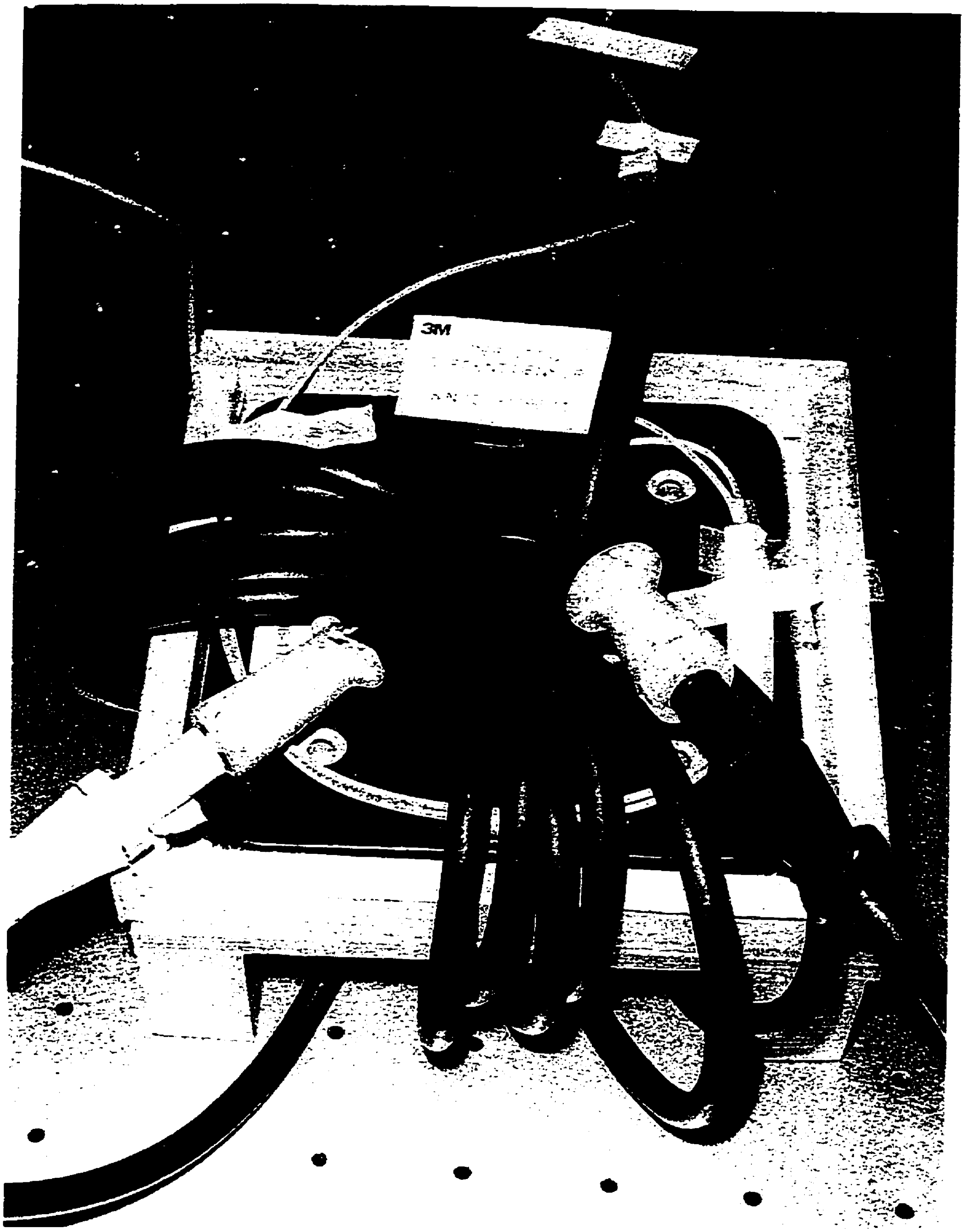

Figure 6.2. The Current Sensor

taken as a change in the current being measured, a very stable laser transmitter was built with the help of TRLabs, Edmonton. It had an adjustable output and a knob was provided to control the laser drive current which changed the optical power output smoothly. Measurements were made to see the effect of the laser current on its output power and Fig. 6.3 shows that relationship. To characterize the stability of the laser its output was recorded over five hours and readings taken at an interval of one minute. The result is shown in Fig. 6.4 and it can be seen that the laser output is stable over a certain period of time but shows some sudden changes at other times. The output polarization characteristics of the laser were also measured to determine the orientation of the laser output. As shown in Fig. 6.5 it illustrates a true polarization curve with the exception that the lowest point is not zero. It also shows that the laser output is a mixture of polarized and unpolarized light and the orientation of the polarized light is at 20°. Fig. 6.6 shows the actual laser transmitter and its internal circuitry.

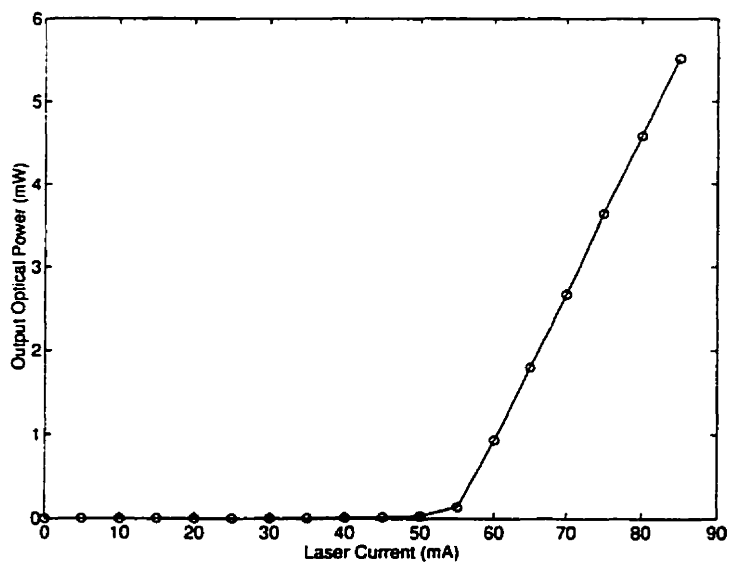

Figure 6.3. The Laser Output Power vs. Laser Current

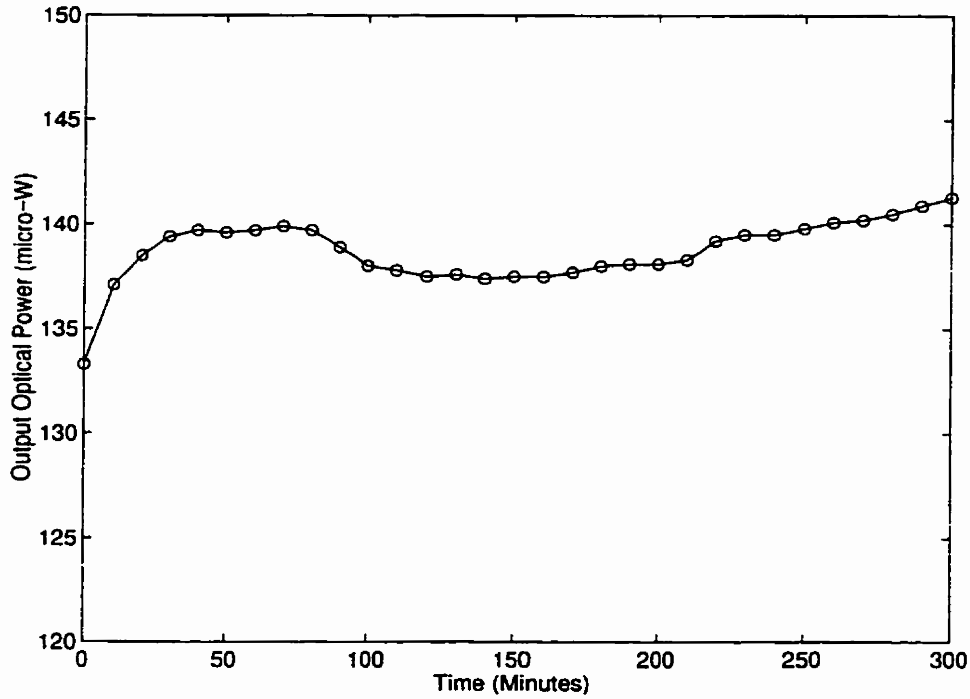

Figure 6.4. The Laser Stability Characteristics

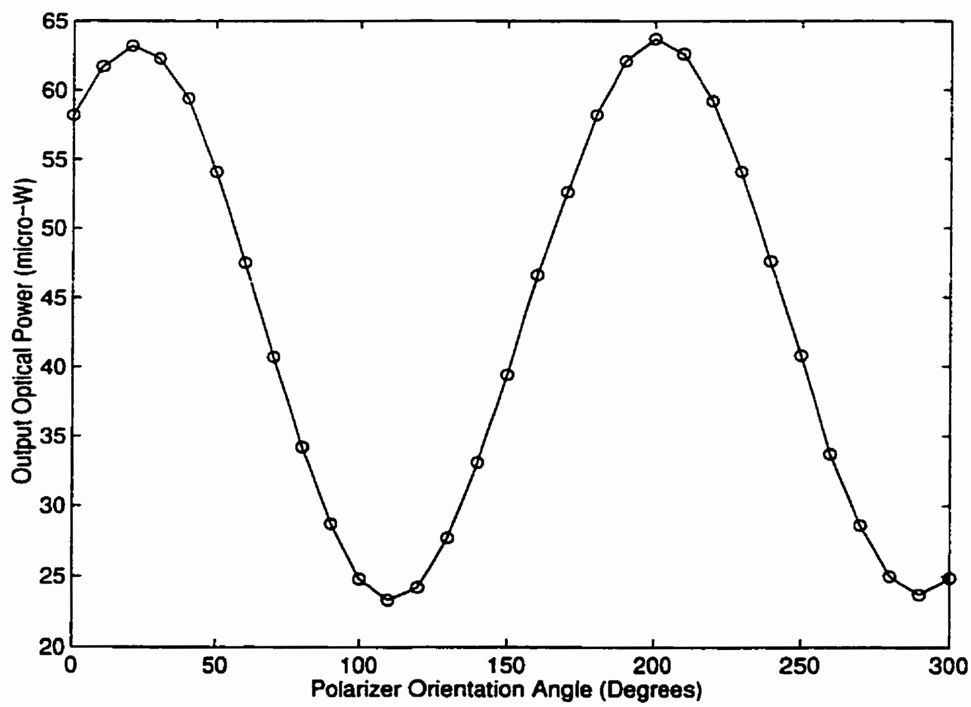

Figure 6.5. The Laser Output Polarization Characteristics

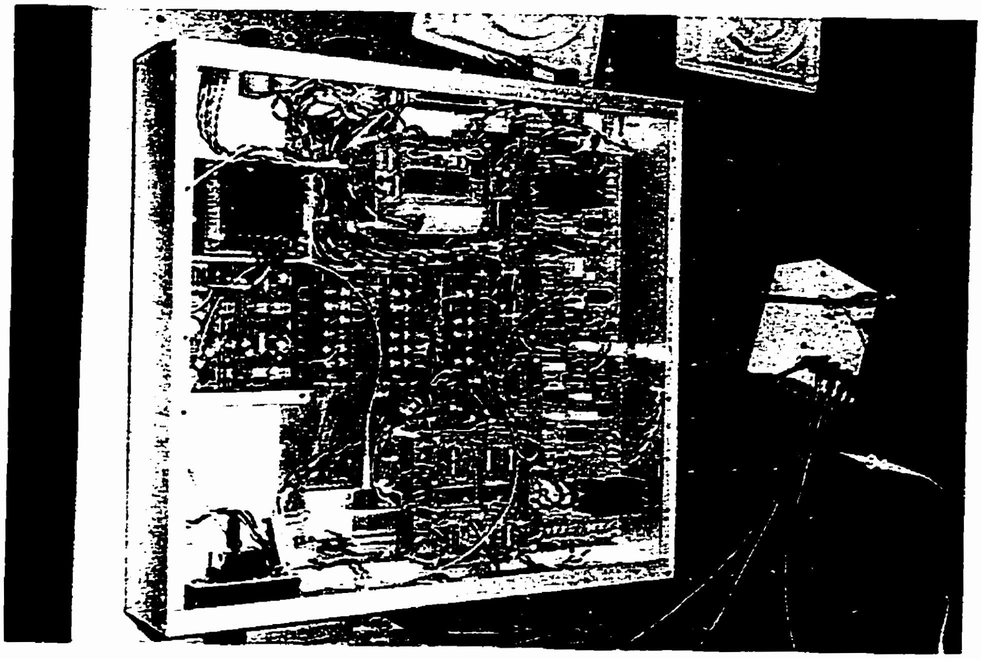

(a)

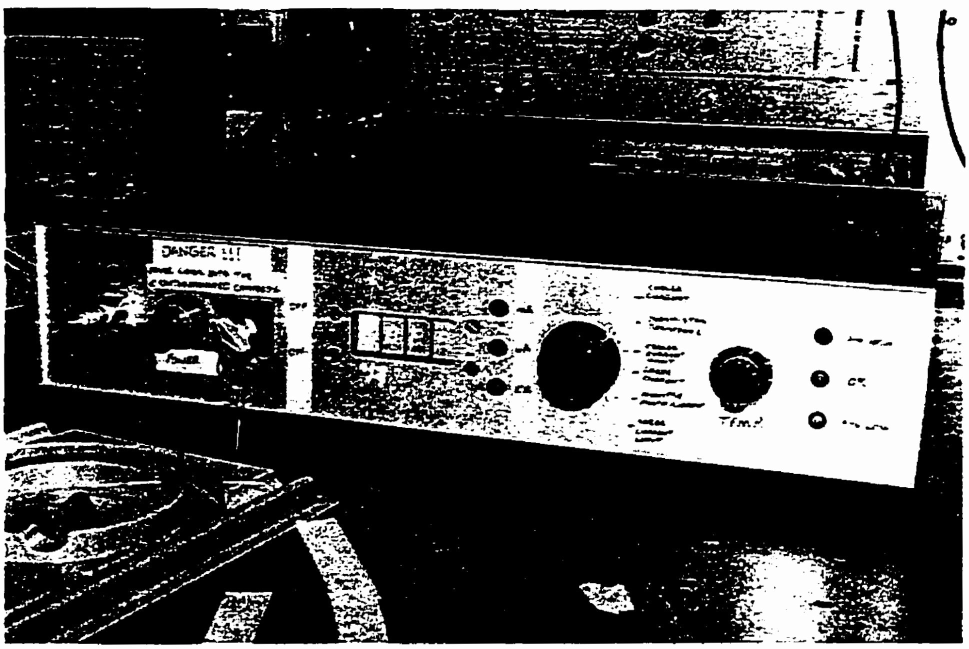

(b)

Figure 6.6. (a) Interior circuit of the laser; (b) Laser box and its control panel

6.3 Optical DC Current Sensing Experiment

Before putting together the fiber optic network it was important to characterize the response of the two current sensors individually. For this each sensor was connected directly between the laser and the optical meter and the laser was operated in the continuous mode i.e. it was not modulated by any pulse. The effective power line D.C. current was increased from 0 to 1400 A in steps of 140 A and the change in the optical meter reading was observed. Both the sensors demonstrated highly linear relationships as a function of the current being measured though their slopes were slightly different. Figs. (6.7 and 6.8) show the intensity change relationship w.r.t. the line current for the sensors 1 and 2 respectively.

The next set of readings were taken with the laser being operated in the pulsed mode. the modulation pulses being generated by the Xilinx and only one sensor was tested at a time. These readings also tested the operational performance of the receiver as the output was being displayed on the PC. The values displayed were the digitized values of the analog signal by the analog-to-digital converter which were stored by the Xilinx and then passed on to the DSP which sent them for display to the PC. The values were being sampled and processed every 1.6388 ms. Also displayed on the PC was an average value which was the average of 1024 samples. As, in this case, there was only one pulse coming to the receiver and the receiver system is set up to digitize and display two pulses , the PC displayed '-1' indicating that the differential amplifier did not see any signal from the photodiode for the second pulse. The results of the this experiment are shown in Figs. (6.9 and 6.10) and it can be seen that the results match very closely those obtained with the laser in continuous mode.

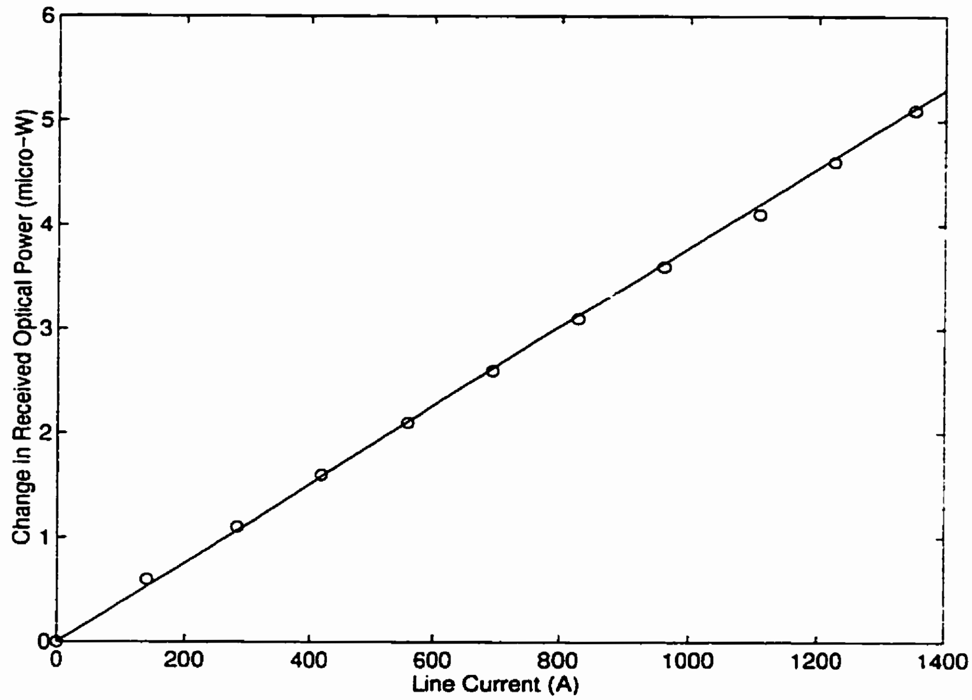

Figure 6.7. C.W. Response of Sensor 1

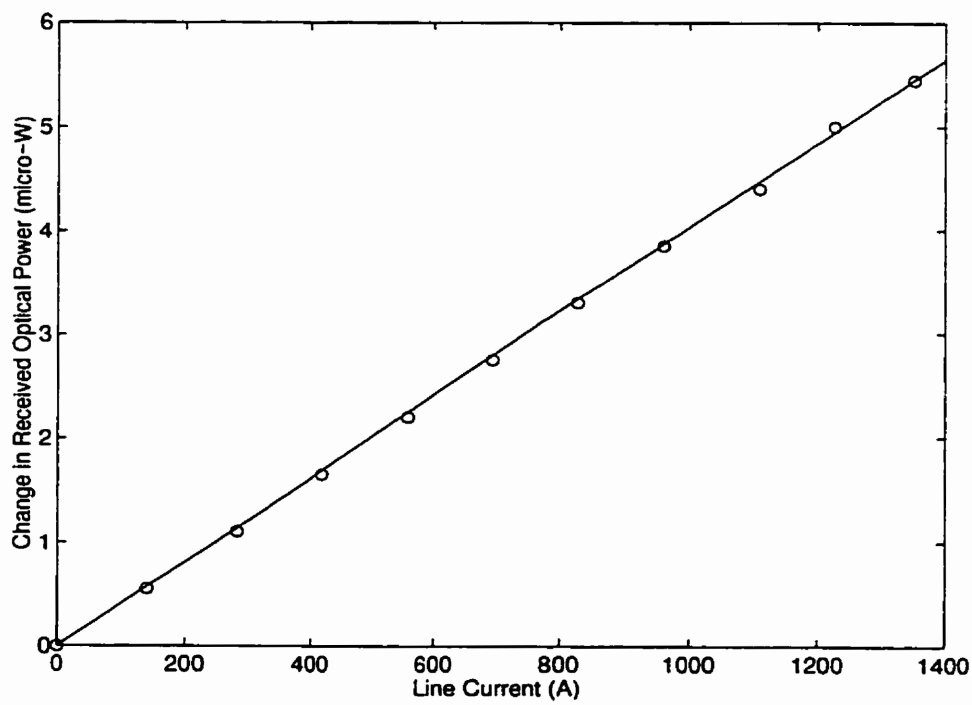

Figure 6.8. C.W. Response of Sensor 2

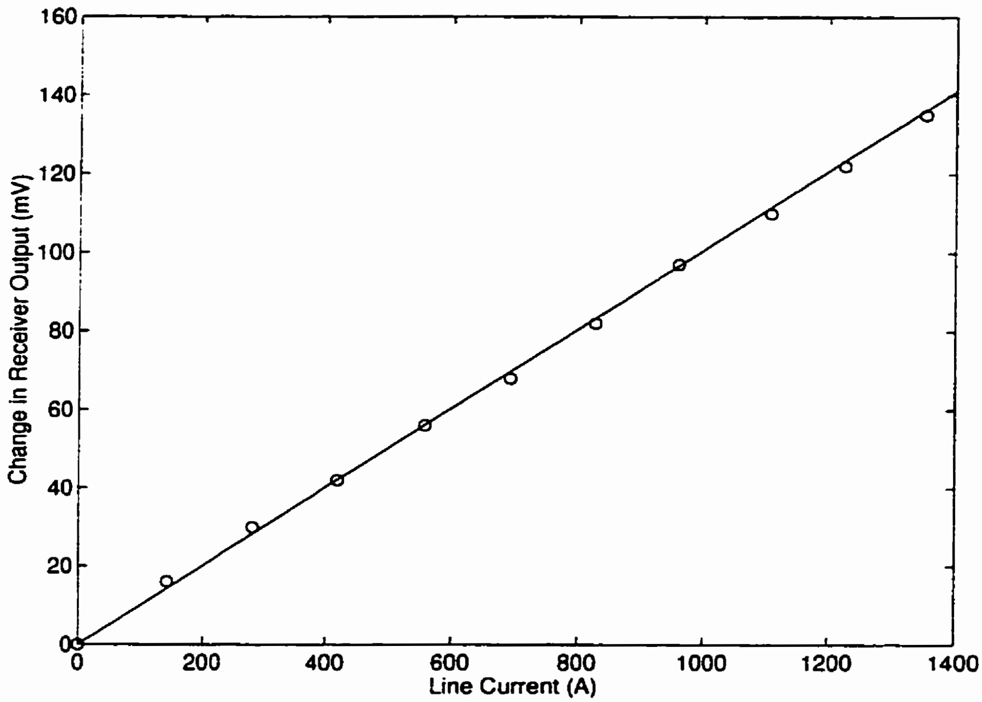

Figure 6.9. Pulsed Response of Sensor 1 with Output on PC

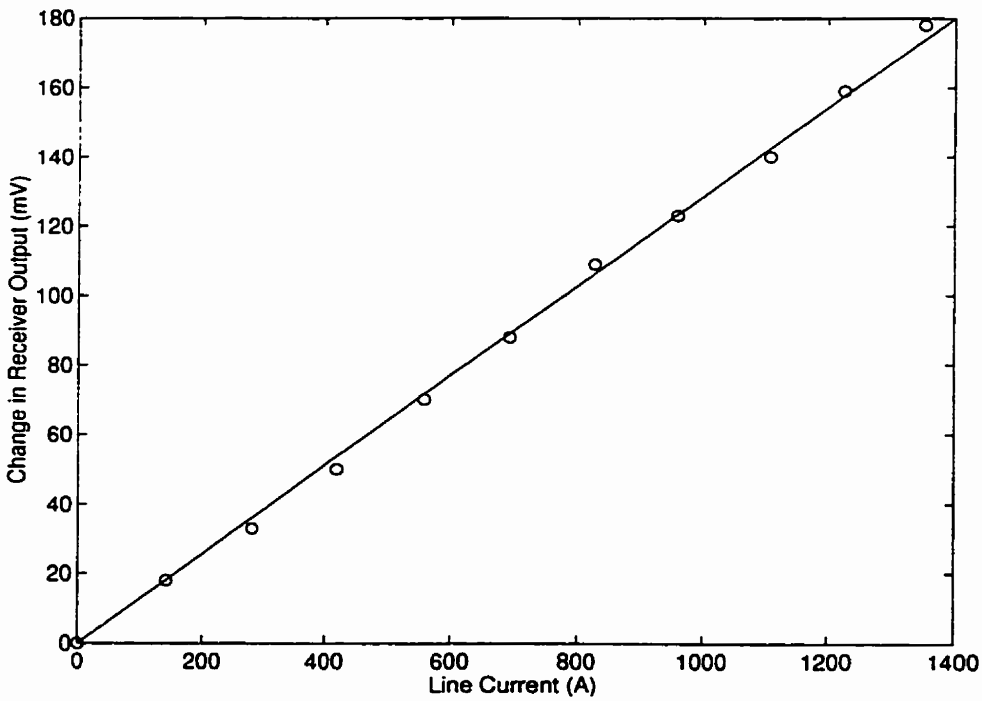

Figure 6.10. Pulsed Response of Sensor 2 with Output on PC

6.4 Networked Current Sensing Experiment

Before putting together the whole network it was necessary to see if the receiver would be able to sample the two pulses and show the output accurately. For this the twin pulses were simulated by using the HP Pulse Generator. It was given a synchronization trigger pulse from the Xilinx and it provided two output pulses whose width, delay and amplitude were adjustable. As the actual pulse width is 400 ns long, the pulse width was set at 400 ns. The pulse amplitudes were then set at different values between 0 and 1 V and the output displayed on the PC monitor observed. The results obtained were highly accurate. The values displayed on the PC monitor followed the actual values as observed on the Digital Oscilloscope very closely within an accuracy range of up to 5 mV. These results demonstrated that the receiver operated as it was designed to do. Fig. 6.11 shows the receiver and its major components.

After making sure that the receiver was functioning properly the stage was set for connecting the entire fiber optic network. The fiber ends which were to be spliced together were stripped and cleaved and then very carefully inserted into the mechanical splice such that their faces gently touched each other and then the splice was locked. All this had to be done extremely carefully as a slight change in their relative positions could result in a high optical loss. The system had a total of six splices, three on each optical path. The complete FOCSNET system is shown in Fig. 6.12.

With the help of the digital scope the time separation between the two pulses and their distance from the trigger pulse were checked. As explained in Chapter 3 the separation between the leading edges of the two pulses should be 800 ns and their

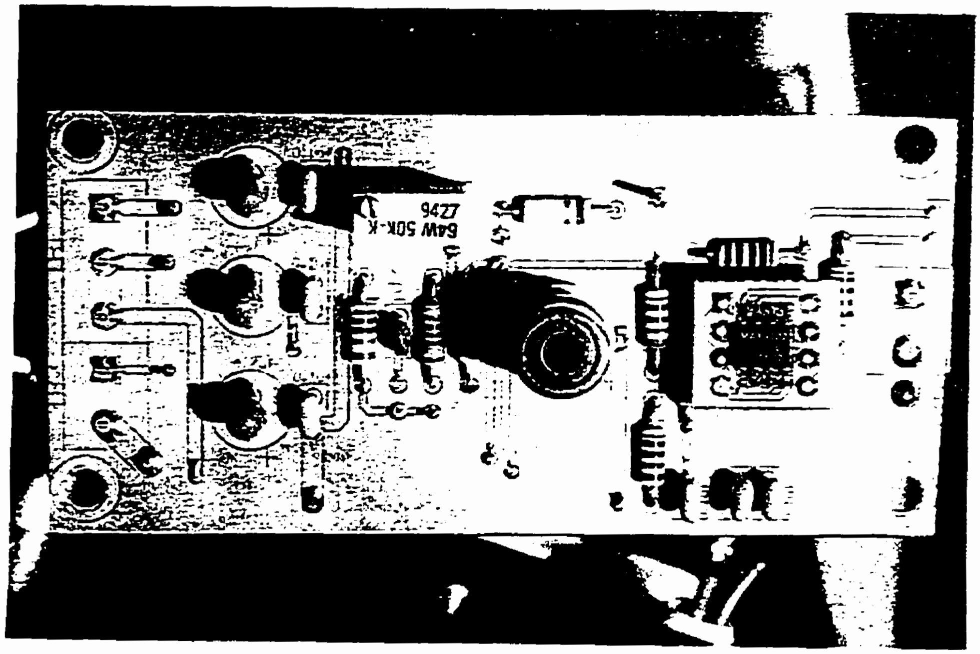

(a)

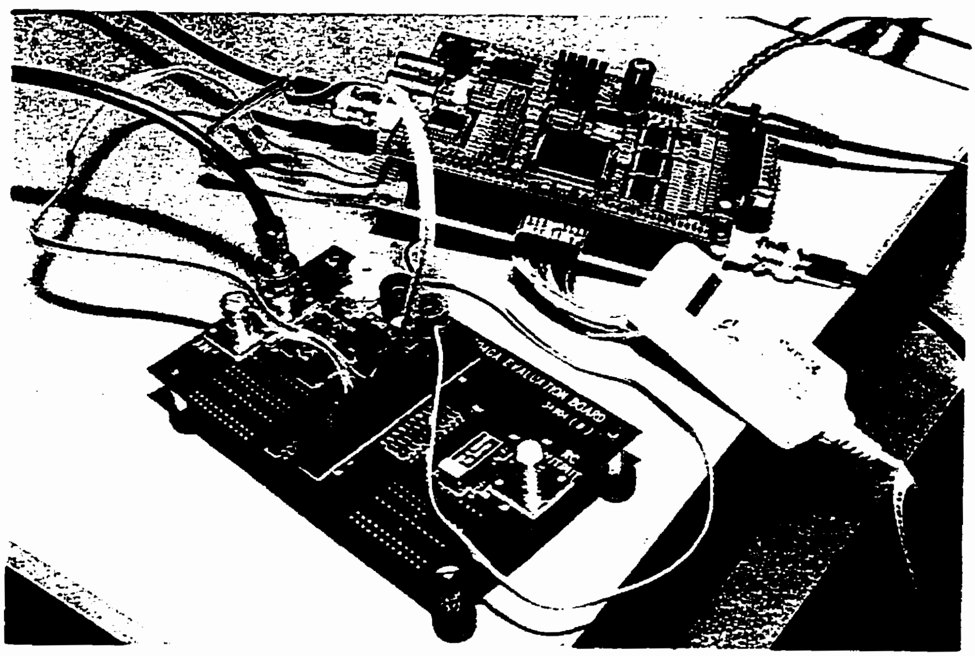

(b)

Figure 6.11. The Receiver (a) Photodiode and Differential Amplifier; (b) ADC, Xilinx and DSP boards

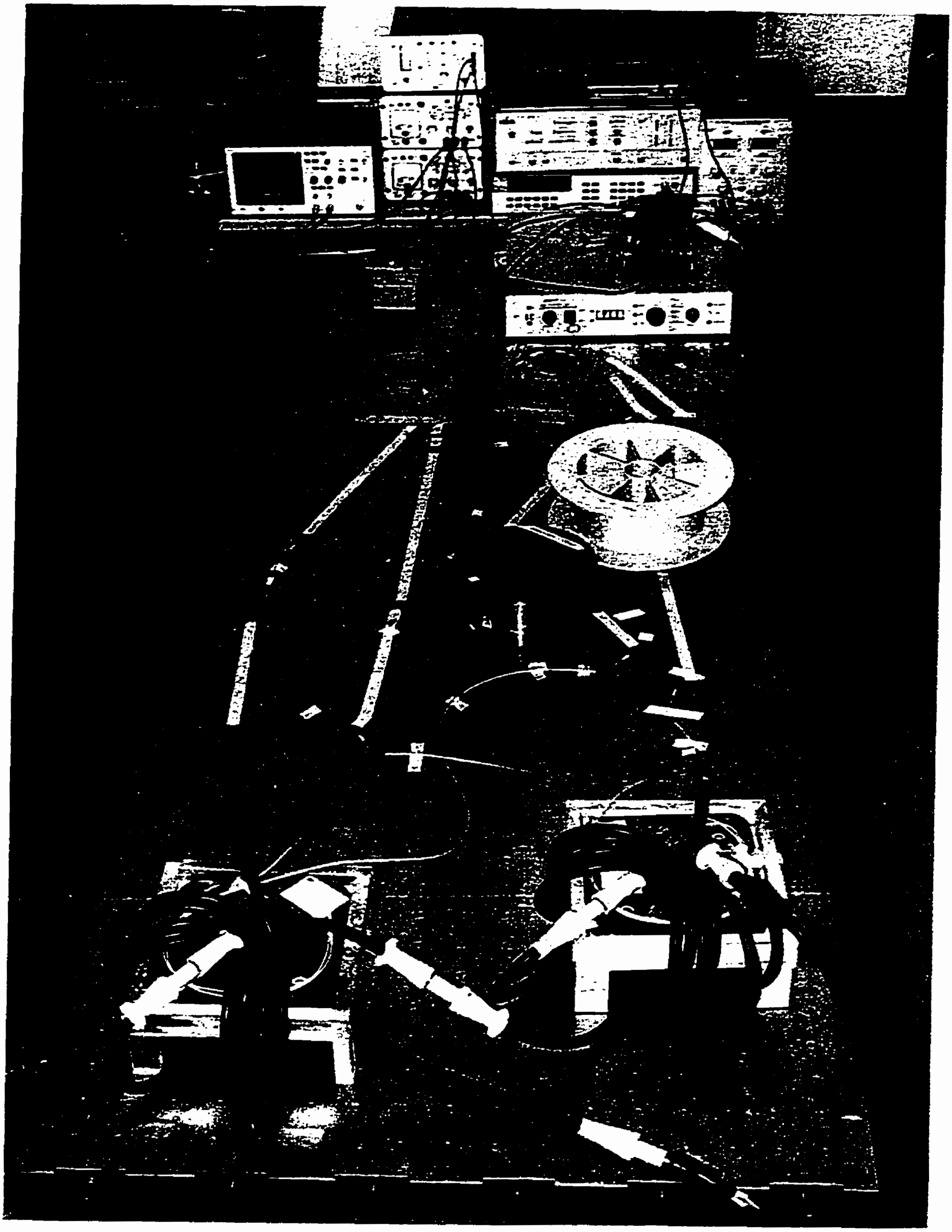

Figure 6.12. Fiber Optic Current Sensor Network System

distance from the trigger pulse should be 50 ns. but the waveforms displayed by the scope were as shown in Fig. 6.13.

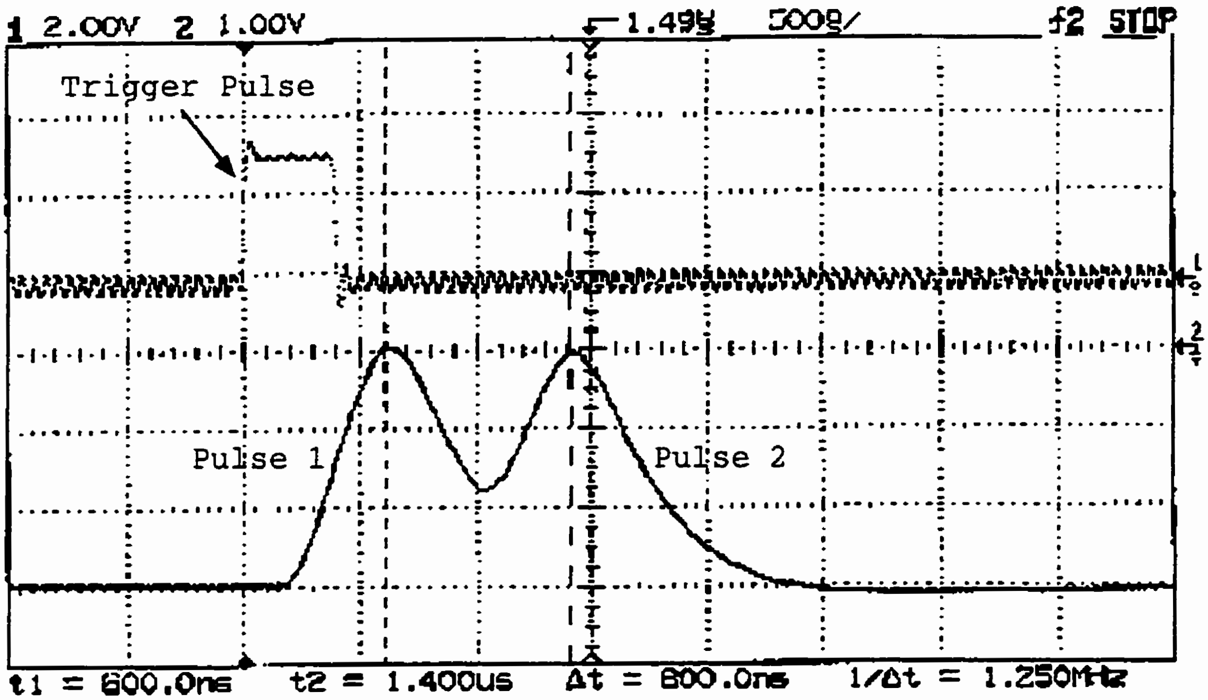

Figure 6.13. Time Separation between the Pulses

As can be seen the output from the differential amplifier that goes to the analog-to-digital converter is not two separate pulses but two peaks which are not entirely separated from each other. The time difference between the peaks is 800 ns as expected but the time gap between the trigger pulse and the first peak is 600 ns instead of 450 ns as expected. This can be explained. in part. due to slower than expected rise and fall times from the photodiode. Though the photodiode is designed to have a high slew rate the slow rise and fall times can be caused by stray and parasitic capacitance due to many factors including the layout of the PCB, long lead lengths etc. Though unexpected this did not pose any difficulty as the sampling times by the analog-to-digital converter could be adjusted using the delay lines as explained in Chapter 4.

To get the output of the networked system on the PC display the delays were adjusted such that the analog-to-digital converter sampled at points 600 ns and 1300 ns away from the leading edge of the trigger pulse. This means that the first pulse is sampled at its peak value whilst the second is sampled 100 ns before its peak value but that was the maximum delay that could be inserted by the delay lines. The output displayed on the PC was fairly close to the actual value but due to the noise present in the optical signal the digitized values of the noisy analog signal were not entirely consistent and the values being displayed on the PC were changing accordingly. The reason for this noise could be the optical noise due to the mechanical splices or badly cleaved fiber ends. Due to this random change the actual shift in the values was difficult to observe so the readings had to be taken with the help of the digital scope. When the line current was switched on the output waveform displayed a rise in its value and Fig. 6.14 shows the increase in the output when 1350 A of D.C. current was passed through both the sensors.

Readings were taken in three different set ups. In the first set up the same amount of current was passed through both the sensors simultaneously and the line current increased in steps of about 140 A. Figs. (6.15 and 6.16) show the response of the two sensors in the first set up. In the second set up the current was passed through only the first sensor and its readings taken. The third set up was similar to the second set up with the exception that this time the current was passed through only the second sensor. Figs. (6.17 and 6.18) show the response of the first and the second sensor, respectively, when the line current is increased in steps of 140 A. The reference value of the line current was measured using a calibrated shunt resistance of 0.5 mΩ in series with the conductor and measuring the voltage across it with an accurate voltmeter.

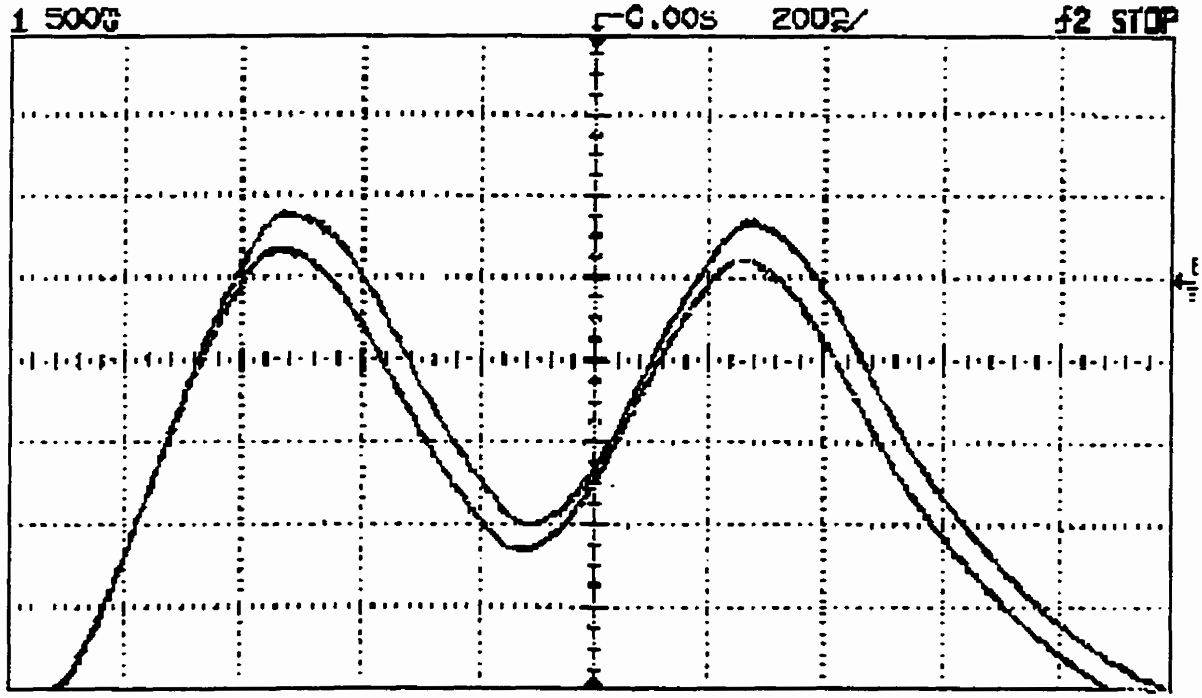

Figure 6.14. Increase in the Output with 1350 A of D.C. Current through both the Sensors

It can be observed from the graphs that the maximum value of the change in the receiver output for the same sensor is different in different graphs. This is due to the fact that these readings were taken at different times which meant that there was a change in the laser power and a slight change in the physical set up resulting in a change in the optical losses and thus a slight variation in the light intensity reaching the receiver.

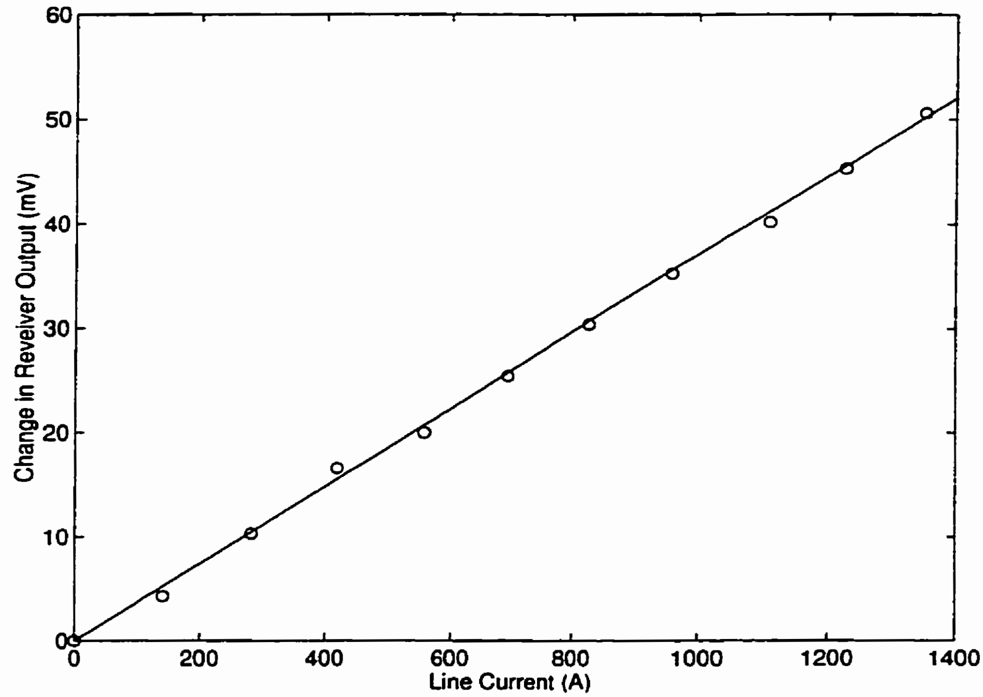

Figure 6.15. Pulsed Response of Sensor 1 with Current through both the Sensors

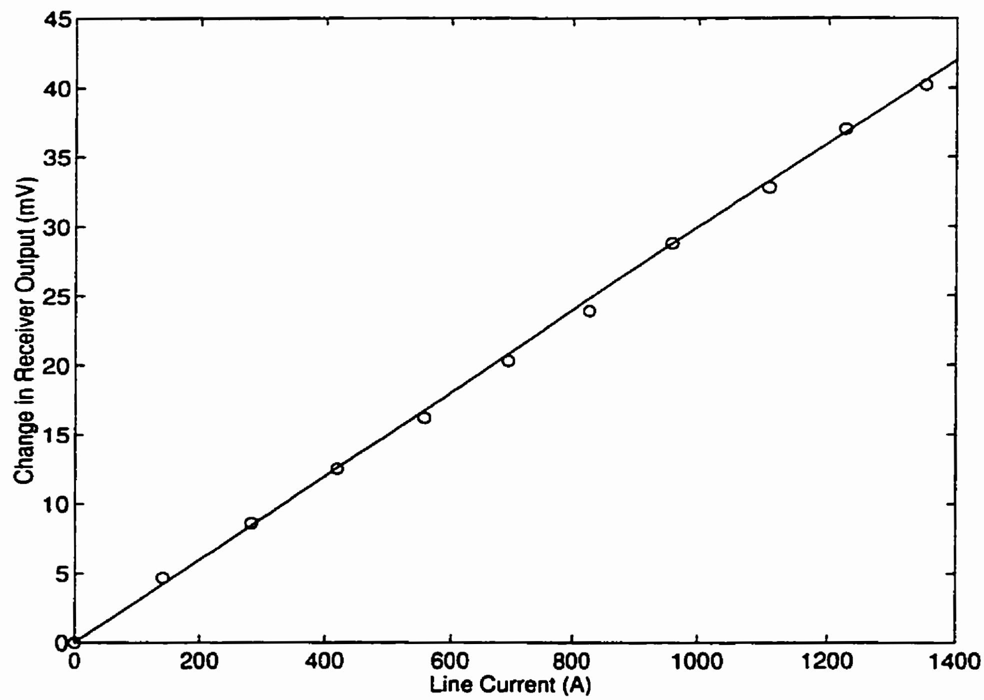

Figure 6.16. Pulsed Response of Sensor 2 with Current through both the Sensors

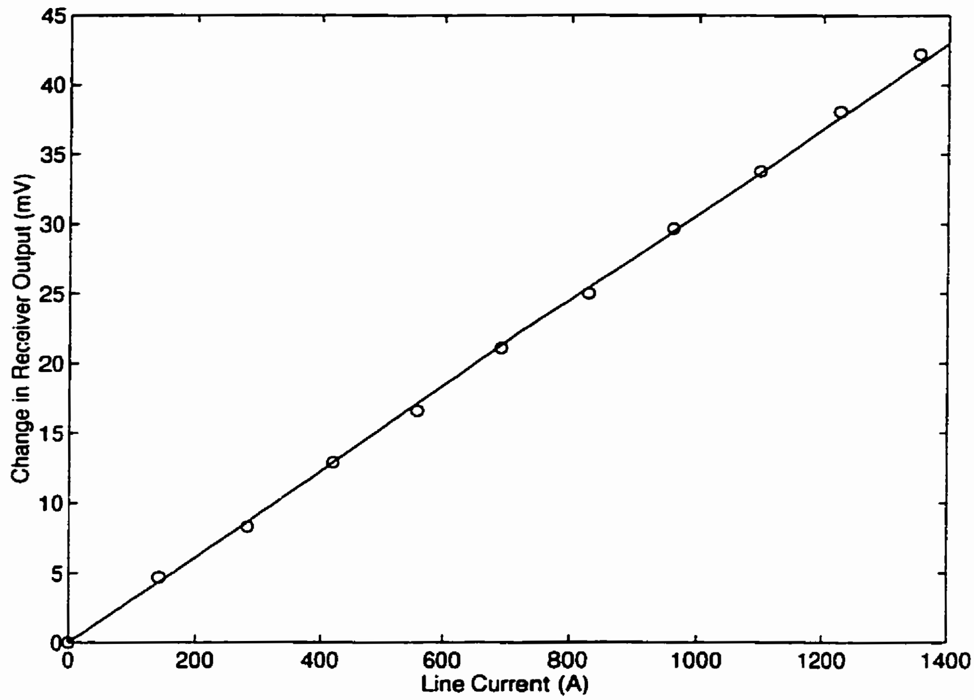

Figure 6.17. Pulsed Response of Sensor 1 with Current passing through it only

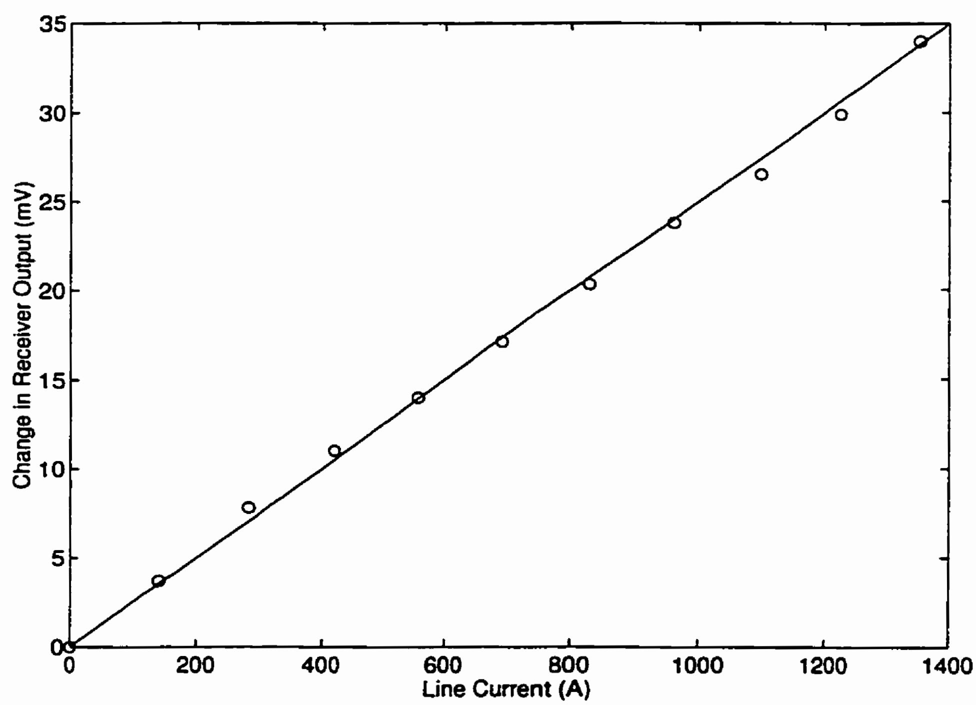

Figure 6.18. Pulsed Response of Sensor 2 with Current passing through it only

To prove conclusively that the system can measure two different currents simultaneously two different currents were passed through the two sensors such that the sum of the two currents always remained at 1355 A. Due to physical laboratory constraints the two currents were changed in steps of 270 A. If the system is working properly then not only should the changes in the receiver output for the two sensors be linear but the sum of the two output changes at any point should also follow a linear relationship. Fig. 6.19 shows the results obtained from this experiment. It can be seen that all the three curves are linear in nature thus proving that FOCSNET can measure different currents simultaneously. It is also observed that the sum of the changes in the two sensor output pulses, though linear, is not a horizontal line and

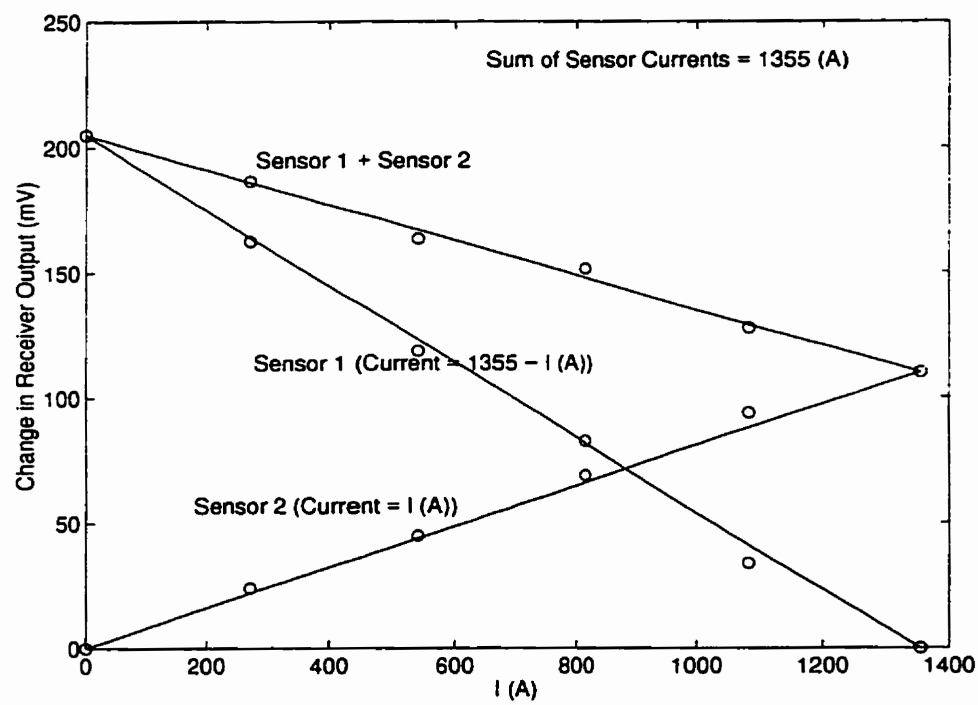

Figure 6.19. Pulsed Response of the System with different Currents passing through the two Sensors

this is due to the fact that the two sensors have different sensitivities i.e. their responsivity curves have different slopes. In fact the curve representing the sum of the sensor currents can be taken as a 'Figure of Merit' for the two sensors in that the less the slope of this curve the more identical the two sensors are in terms of their response. When this line becomes horizontal it would mean that the two sensors are truly identical in performance.

6.5 Analysis of Results

Based on the above experimental results it is concluded that this 'proof of concept' FOCSNET system has been truly successful in its main objective, which was to prove that the 3M optical current sensors can be networked together using a Time Division Multiplexing (TDM) approach. The results also demonstrate that both the current sensors have a highly linear response. The experiments also brought to light the effect of optical noise, due in part to bad splicing, on the system and the need for a better technique like fusion splicing.

CHAPTER 7

CONCLUSIONS AND FUTURE WORK

In this work a proof of concept fiber optic current sensor network using a time division multiplexing approach has been implemented. The Laser diode transmitter capable of providing very short, high power optical pulses was specifically constructed for this project as was the receiver which consists of photodiode, operational amplifier, analog-to-digital converter, Xilinx, digital signal processor and a PC. The experimental investigation of the simultaneous sensing of two different D.C. currents was successfully conducted.

The polarization properties of light and the principles of the optical current sensor based on the Faraday magneto-optic effect were analyzed theoretically and the working of a fiber optic current sensor wound around the current carrying conductor and having a single detection scheme were discussed.

Various network topologies and multiplexing schemes were compared in terms of cost, complexity of design, construction time, flexibility, system losses etc. Based upon such comparisons a passive Star network using a TDM approach was selected and various parameters like fiber lengths and the pulse width were then determined.

The receiver which consists of many different components interlinked with each other was designed and built. The photodiode converted the optical signal to an electric signal and this signal was fed to a differential amplifier so that only the part of signal containing the change in intensity was amplified. This voltage signal was then converted to a digital signal by the analog-to-digital converter (ADC). This digital data was fetched and stored by the Xilinx and given to the digital signal processor for processing. The DSP sent each data signal it received as well as the average of the 1024 signals to PC for display. The overall receiver functioning was tested by simulating the light pulses using a pulse generator and feeding its output directly to the ADC. The receiver was able to measure the amplitude of the pulses very accurately. within an accuracy range of up to 5 mV.

Finally the experiments on current sensing were successfully conducted. First the experiments were conducted using single sensors in order to fully characterize the behaviour of the two sensors. These experiments were conducted with a continuous laser beam as well as a pulsed laser and using the PC display for a current range of 0 A to 1400 A of DC current. Though both the 3M sensors show highly linear curves with slightly different slopes it was amply demonstrated that the receiver can measure different currents simultaneously.

It should be noted that due to the limitations of the available power supplies the system could be tested only up to a maximum equivalent current of around 1400 A. In spite of the system being non-optimum it proved to be remarkably rugged and in fact its performance. as a proof of concept experiment. exceeded expectations. With improvements to the fiber splicing, and especially the receiver design. the sensitivity performance of the FOCSNET system can be improved very considerably.

Future work will involve improving the stability of the light source. Stability of the light source is extremely important in this system since any change in the input optical power can be inferred as the presence of some line current. Work will be done to design some kind of feedback system so that the accurate determination of the line current remains effectively immune to any change in the source optical power.

It was observed during the experiments that there was a considerable amount of optical noise at the receiver. This could have been due in part to bad splicing as the splices used were mechanical splices and improperly cleaved fiber ends may also have played their part. Very high quality cleavers and fusion splicing can be used to reduce such optical noise.

Improvements can definitely be made in the design of the photodiode/amplifier circuit and the layout of the PCB as the two optical pulses which were 400 ns wide and separated by a 400 ns gap should not have the shape and such a large rise and fall times as were observed with the present set up. The two optical pulses are clearly isolated from each other and the converted electrical signal should have virtually the same shape as that of the optical signal that the photodiode receives.

A lot of changes can be made in the DSP software and the Xilinx design to make this system more general. The present system is designed for only two sensors but it has been designed to be easily modified.based upon an input to the system through the computer by the user, such that the receiver will operate for any number of sensors. Also work can be done to reduce the pulse width and the separation as much as possible in order for the system to detect very fast transient currents. This would most probably require a very fast response from the ADC, DSP, PC and the photodiode circuit. Modifications can also be made to the DSP software so that instead of averaging 1024 values, it determines the maximum value of the A.C. signal thus providing the capability to measure AC currents. The system is well configured to distinguish between AC and DC currents, except that a number of changes in the software are required.

The transmitter should also be replaced by a high power LED since, apart from the cost, it also has better output polarization properties than the laser diode.

REFERENCES

[1] J.R. Boyle, et al, "The Tennessee Valley Authority's (TVA's) experience and action plans with freestanding oil-filled current transformers (CTs)", *IEEE Transactions on Power Delivery*, vol. PWRD-3, No. 4, October 1988, pp. 1769-1775.

[2] IEEE power system relay committee, "Gapped core current transformer characteristics and performance", *IEEE Transactions on Power Delivery*, vol. PWRD-5, No. 4, November 1990, pp. 1732-1740.

[3] H. Schwarz and M. Hudasch, "Optical current transformers-successful first field test in a 380 kV system", *ABB Review*, March 1994, pp. 12-18.

[4] M. Kanoi, G. Takahashi, T. Sato, M. Higaki, E. Mori and K. Okumura, "Optical voltage and current measuring system for electric power systems", *IEEE Transactions on Power Delivery*, vol. PWRD-1, January 1986, pp. 91-97.

[5] A.J. Rogers, "Principles for optical-fibre applications in electricity supply", *Journal of Optical Sensors*, vol. 1,January 1986, pp. 5-25.

[6] A. Papp and H. Harms, "Magneto-optical current transformer", *Applied Optics*, vol. 19, November 1980, pp. 3729-3745.

[7] T. Mitsui, K. Hosoe, H. Usami and S. Miyamoto, "Development of fiber optic voltage sensors and magnetic field sensors", *IEEE Transactions on Power Delivery*, vol. PWRD-2, January 1987, pp. 87-93.

[8] E.A. Ulmer Jr., "A high accuracy optical current transducer for electric power systems", *IEEE Transactions on Power Delivery*, vol. PWRD-5, April 1990, pp. 892-898.

[9] G.W. Day and A.H. Rose, "Faraday Effect Sensors: The State of the Art", *Proc. SPIE*, vol. 985, 1988, pp. 1-13.

[10] Y.N. Ning, Z.P. Wang, A.W. Palmer, K.T.V. Grattan and D.A. Jackson, "Recent progress in optical current sensing techniques", *Review of Scientific Instruments*, vol. 66, No. 5, May 1995, pp. 3097-3111.

[11] P.-G. Zhang and D. Irvine-Halliday, "Faraday Effect Optical Current Sensor", *CCECE '96*, pp. 871-875.

[12] T.W. MacDougall, J.W. Dawson and E. Hernandez, "State of the Art Fiber Optic Current Sensor", *OFS*, 1996.

[13] T.W. Cease and P. Johnson, "A magneto-optical current transducer", *IEEE Transactions on Power Delivery*, vol. PWRD-5, No. 2, April 1990, pp.548-555.

[14] S. Kobayashi, A. Horide, I. Takagi, M. Higaki, G. Takahashi, E. Mori and T. Yamagiwa, "Development and field test evaluation of optical current and voltage transformers", *IEEE Transactions on Power Delivery*, vol. PWRD-7, No. 2, April 1992, pp. 815-821.

[15] Jun Song, "Development of Magneto-optical Current Transducers for Power Systems", Ph.D. Thesis, University of Manitoba, January 1996.

[16] Peng-Gang Zhang, "Faraday Effect Optical Current Sensor", Master's Thesis, University of Calgary, August 1993.

[17] T. Fujimoto, M. Shimizu and H. Nakagawa, "Development of an Optical Current Transformer for Adjustable Speed Pumped storage Systems", *IEEE Transactions on Power Delivery*, vol. 12, No. 1, January 1997, pp. 45-50.

[18] T. Yoshino, "Optical fiber sensors for electric industry", *Fiber Optic Sensors II, SPIE*, 1987, pp. 258-265.

[19] T.W. MacDougall, D.R. Lutz and R.A. Wandmacher, "Development of a fiber optic current sensor for power systems", *IEEE Transactions on Power Delivery*, vol. PWRD-7, No. 2, April 1992, pp. 848-852.

[20] P. Menke and Th. Bosselmann, "Magnetooptical AC-current sensing with an annealed fibre coil and intrinsic temperature compensation", *Proc. SPIE*, vol. 2292, 1994, pp. 26-33.

[21] Andreas Koch, Holger Hirsch, Dirk Peier and Hartwig Senftleben, "Fiber optic current transformer with low cost standard connectors employing a fibre depolariser", *Proc. SPIE*, vol 2510, 1995, pp. 224-233.

[22] J.W. Dawson, T.W. MacDougall and E. Hernandez, "Verdet Constant Limited Temperature Response of a Fiber-Optic Current Sensor", *IEEE Photonics Technology Letters*, vol. 7, No. 12, December 1995, pp. 1468-1470.

[23] B. Culshaw and J.P. Dakin, *Fiber Optic Sensors, Volume II, Systems and Applications*, Artech House, London and Norwood, 1988.

[24] A.R. Nelson and D.H. McMahon, "Passive Multiplexing Techniques for Fiber Optic Sensor Systems", *Proc. IFOC*, March 1981, pp. 27-30.

[25] J. Mlodzianowski, D. Uttamchandani and B. Culshaw, "A Simple Frequency Domain Multiplexing System for Optical Point Sensors", *Journal of Lightwave Technology*, vol. 5, No. 7, July 1987, pp. 1002-1007.

[26] B. Culshaw, "Fibre optic sensor networks", *Proc. SPIE*, vol. 1511, 1991, pp. 168-175.

[27] M. Kuribara and M. Kurono, "Passive optical multipoint sensing system for voltage measurement", *IEE Proceedings*, vol. 136, Pt. T, No. 6, December 1989, pp. 315-318.

[28] J.L. Brooks, R.H. Wentworth, R.C. Youngquist, M. Tur, B.Y. Kim and H.J. Shaw, "Coherence Multiplexing of Fiber-Optic Interferometric Sensors", *Journal of Lightwave Technology*, vol. 3, No. 5, October 1985, pp. 1062-1071.

[29] M. Farhadiroushan and R.C. Youngquist, "Polarimetric coherence multiplexing using high-birefringence optical-fiber sensors and short coherence sources", *Optics Letters*, vol. 15, No. 14, July 15, 1990, pp. 786-788.

[30] C. Yeh, *Handbook of fiber optics*, Academic Press Inc., 1988.

[31] D. Clarke and J.F. Grainger, *Polarized Light and Optical Measurement*, Pergamon Press, 1971.

[32] W.A. Shurcliff and S.S. Ballard, *Polarized Light*, D. Van Nostrand Company, Inc., 1964.

[33] R.C. Jones, " A New Calculus for the Treatment of Optical Systems", *J. Opt. Soc. Am.*, vol. 31, July 1941, pp. 488-493. Reprint found in " Polarized Light", *Benchmark Papers in Optics*, vol. 1, Dowden, Hutchinson and Ross, Inc., 1975, pp. 187-192.

[34] M. Faraday, " Experimental Researches in Electricity", *Philosophical Transactions of 1846-1852*, Bernard Quaritch, 1855, pp. 1-26. Reprint found in " Polarized Light", *Benchmark Papers in Optics*, vol. 1, Dowden, Hutchinson and Ross, Inc., 1975, pp. 104-123.

[35] A.M. Smith" Polarization and magneto-optic properties of single-mode optical fiber", *Applied Optics*, vol. 17, No. 1, January 1978, pp. 52-56.

[36] S.C. Rashleigh, " Origins and control of polarization effects in single-mode fibers", *Journal of Lightwave Technology*, vol. 1, No. 2, 1983, pp. 312-331.

[37] J.M. Senior, *Optical fiber Communications*, 2nd Ed., Prentice Hall Inc., 1992.

[38] M.R. Khan, " Measurement of beat length in high birefringent fibers using Faraday magneto-optic effect", Master's Thesis, University of Calgary, June 1996.

[39] Oz Optics Ltd., *Polarization Maintaining Fiber Optic Components*, 1995.

[40] J. Noda, K. Okamato and Y. Sasaki, " Polarization-Maintaining Fibers and their Applications", *Journal of Lightwave Technology*, vol. 4, No. 8, August 1986, pp. 1071-1089.

[41] J.R. Simpson, R.H. Stolen, F.M. Sears, W. Pleibel, J.B. MacChesney and R.E. Howard, " A single-polarization fiber", *Journal of Lightwave Technology*, vol. 1, No. 2, 1983, pp. 370-373.

[42] M.J. Messerly, J.R. Onstoff and R.C. Mikkelson, " Broad-band single polarization optical fiber", *Journal of Lightwave Technology*, vol. 9, No. 7, July 1991, pp. 817-820.

[43] A.H. Rose, Z.B. Ren and G.W. Day, " Twisting and Annealing Optical Fiber for Current Sensors", *Journal of Lightwave Technology*, vol. 14, No. 11, November 1996, pp. 2492-2497.

[44] R.I. Laming and D.N. Payne, "Electric Current Sensors Employing Spun Highly Birefringent Optical Fibers", *Journal of Lightwave Technology*, vol. 7, No. 12, December 1989, pp. 2084-2094.

[45] D. Tang, A.H. Rose, G.W. Day and S.M. Etzel, " Annealing of Linear Birefringence in Single-Mode Fiber Coils: Application to Optical fiber Current Sensors", *Journal of Lightwave Technology*, vol. 9, No. 8, August 1991, pp. 1031-1037.

[46] A.H. Rose, S.M. Etzel and C.M. Wang, " Verdet Constant Dispersion in Annealed Optical Fiber Current Sensors", *Journal of Lightwave Technology*, vol. 15, No. 5, May 1997, pp. 803-807.

[47] J. Graeme, *Photodiode Amplifiers*, McGraw-Hill, 1995.

[48] EG&G Optoelectronics, *Silicon Photodiodes*, 1992.

TEST TARGET (QA-3)

150mm

6"

APPLIED IMAGE . Inc
1653 East Main Street
Rochester, NY 14609 USA
Phone: 716/482-0300
Fax: 716/288-5989